Supporting Information

Precise Nanochemistry of Spherical Aluminum Oxo Clusters for Accurate Surface Guest Recognition and Release

Si-Hao Shen, [1, 2] Ying-Hua Yu, [1, 2] Jian-Bing Chen, [1, 3] Wei-Hui Fang *[1] and Jian Zhang *[1]

[1]State Key Laboratory of Structural Chemistry, Fujian Institute of Research on the Structure of Matter, Chinese Academy of Sciences, Fuzhou, Fujian 350002, P. R. China.
[2]University of Chinese Academy of Sciences, Chinese Academy of Sciences, Beijing 100049, P. R. China.
[3]School of Physical Science and Technology, ShanghaiTech University, Shanghai 201210, P. R. China.
*Correspondence: fwh@fjirsm.ac.cn; zhj@fjirsm.ac.cn

Content

1. Experimental Section.

Chemicals and Materials: All the reagents and solvents employed are purchased commercially and used as received without further purification. Aluminum isopropoxide ($Al(O^iPr)_3$), probenecid and imidazole were acquired from Aladdin Chemical Reagent Shanghai. Lead nitrate ($Pb(NO_3)_2$), isopropyl alcohol (HO^iPr), and *N,N*-dimethylformamide (DMF) were bought from Sinopharm Chemical Reagent Beijing. 1,4-Dioxane, dimethyl sulfoxide (DMSO), benzene, mesitylene, 2,6-dichlorotoluene, anisole, phenylboronic acid pinacol ester, pyrazine, 7-azaindole, 4,4'-bipyridine, 4,4'-vinylenedipyridine, 4,4'-trimethylenedipyridine, and tetrabutylammonium salts, such as tetrabutylammonium nitrate, tetrabutylammonium perchlorate, tetrabutylammonium triflate, tetrabutylammonium tetrafluoroborate and tetrabutylammonium bis((trifluoromethyl)sulfonyl)amide etc., were purchased from Adamas-beta. Lead salicylate and terpineol (mixture of isomer) were purchased from Macklin.

Energy dispersive spectroscopy (EDS): The EDS analyses of single crystals were performed on a JEOL JSM6700F field-emission scanning electron microscope equipped with an Oxford INCA system.

Fourier Transform Infrared (FT-IR) Spectroscopy: FT-IR spectra were collected on a Bruker VERTEX 70 Spectrometer using attenuated total reflection (ATR) ranging from 400 cm^{-1} to 4000 cm^{-1}.

Powder X-ray diffraction (PXRD): PXRD data were performed using a Rigaku Miniflex600 diffractometer with Cu Kα radiation (λ = 1.54056 Å) collected with the angular range (2θ) from 5° to 50° at 298 K.

UV-vis spectroscopy:

The UV-vis diffuse reflection data were recorded at room temperature using a powder sample with $BaSO_4$ as a standard (100% reflectance) on a PerkinElmer Lamda-950 UV spectrophotometer and scanned at 200-800 nm. The absorption data are calculated from the Kubelka-Munk function, ($F(R) = (1-R)^2/2R$), where R representing the reflectance.

High Resolution Electrospray Ionization Mass Spectra (ESI-MS):

The dissolved samples used for ESI-MS measurements are firstly filtered through membrane filter and diluted, then pumped in Impact II Q-TOP mass spectrometer. The experimental peaks were simulated by DataAnalysis software.

General methods for X-ray Crystallography: Crystallographic data were collected on a Rigaku Synergy Custom (Liquid MetalJet D2+) diffractometer with Ga K*α* radiation (λ = 1.3405 Å). The structures were solved with direct methods using $OLEX^2$ and refined by full-matrix least-squares on F^2 using *SHELXTL*. All hydrogen atoms were theoretical hydrogenation, riding on the relevant atoms and refined with fixed thermal factors. Non-hydrogen atoms were refined anisotropically. All absorption corrections were performed using the multi-scan program.

2. Synthesis and characterization.

Synthesis of $Al_{12}Pb_2(O^iPr)_{10}(\mu_2\text{-}O^iPr)_{12}(\mu_2\text{-}OH)_2(\mu_3\text{-}O)_6(\mu_5\text{-}O)_2$. $Al(O^iPr)_3$ (0.500 g, 2.45 mmol), Lead(Ⅱ) salicylate (0.144 g, 0.3 mmol), imidazole (0.068 g, 1 mmol) and tetrabutylammonium nitrate (0.100g, 0.3 mmol) were dissolved in HO^iPr (8 mL) at room temperature. The resultant solution was heated at 80 °C for seven days. After cooling to room temperature, colorless block crystals of were obtained (yield: 5%, based on $Al(O^iPr)_3$). Selected IR peaks (cm^{-1}): 1358 (m), 850 (w), 511 (s). Crystals of **$Al_{12}Pb_2$** are unstable in air and easily weathered, making it impossible to characterize it by powder X-ray diffraction.

Reaction equation of $Al_{12}Pb_2$: $\underline{12Al(O^iPr)_3 + 2Pb(Sal) + 10H_2O + 4IM \rightarrow Al_{12}Pb_2(O^iPr)_{10}(\mu_2\text{-}O^iPr)_{12}(\mu_2\text{-}OH)_2(\mu_3\text{-}O)_6(\mu_5\text{-}O)_2 + 2[HIM]_2[Sal] + 14HO^iPr}$

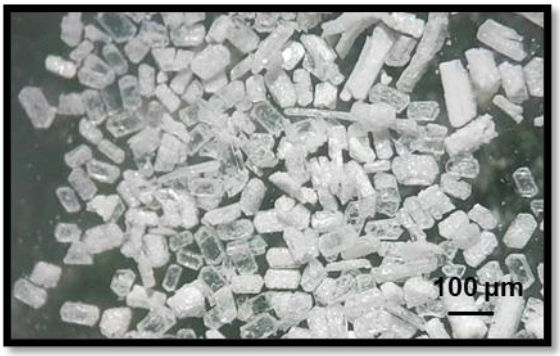

Supplementary Fig. 1. Crystal photograph of **$Al_{12}Pb_2$**.

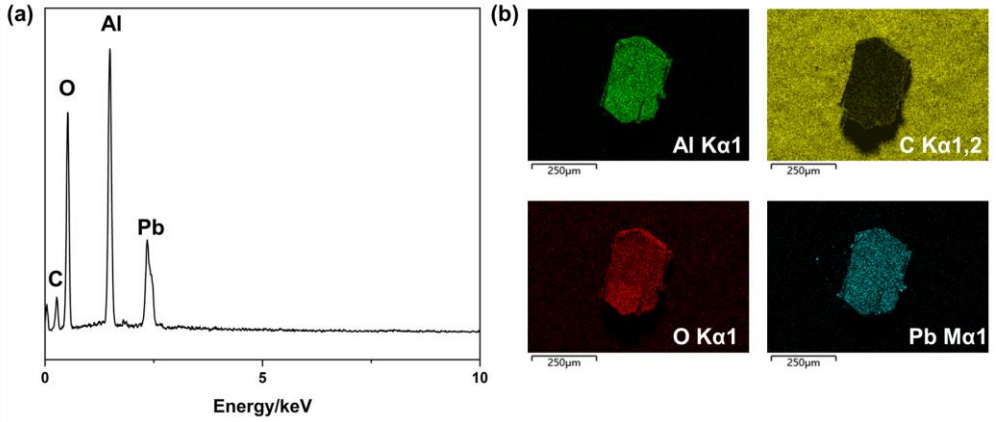

Supplementary Fig. 2. (a) Energy dispersive spectroscopy (EDS) of **$Al_{12}Pb_2$**. (b) EDS mapping of **$Al_{12}Pb_2$**.

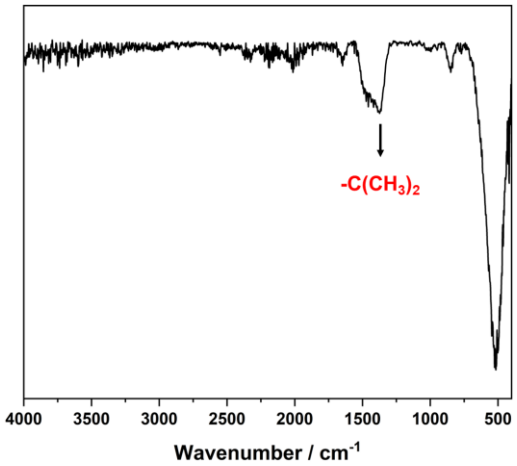

Supplementary Fig. 3. Fourier Transform Infrared (FT-IR) Spectroscopy of **$Al_{12}Pb_2$**.

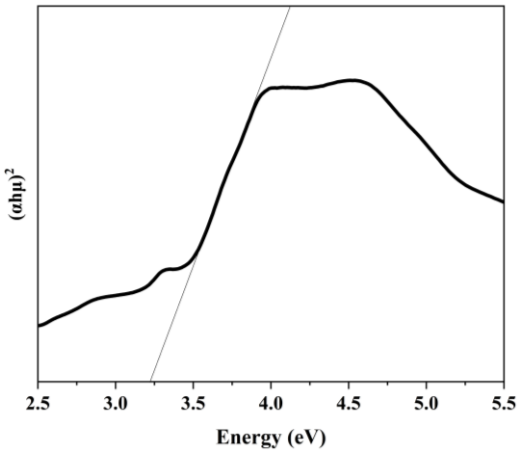

Supplementary Fig. 4. The optical bandgap of **$Al_{12}Pb_2$**.

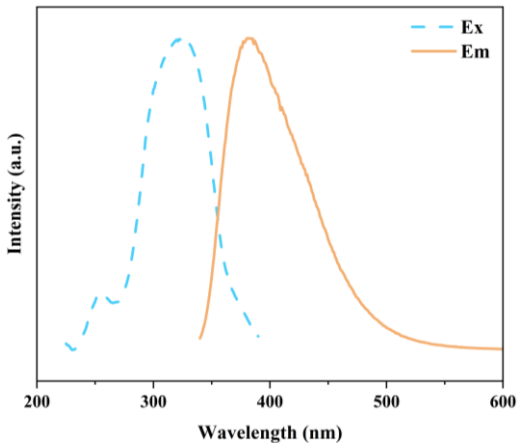

Supplementary Fig. 5. Room-temperature photoluminescence spectra of **$Al_{12}Pb_2$**.

Synthesis of $[Al_{12}Pb_4(BA)_6(O^iPr)_{10}(\mu_2\text{-}OH)_2(\mu_3\text{-}O)_8(\mu_4\text{-}O)_4]^{2+}\cdot 2[NO_3]^-$ (BA = benzoic acid). $Al(O^iPr)_3$ (0.204 g, 1 mmol), benzoic acid (0.122 g, 1 mmol), $Pb(NO_3)_2$ (0.165 g, 0.5 mmol), imidazole (0.068 g, 1 mmol), tetrabutylammonium nitrate (0.1 g, 0.3 mmol), HO^iPr (4 mL) and DMF (1 ml) were added to a 20 mL sealed glass vial and placed in a preheated oven at 100 °C for at least 7 days. After cooling to room temperature, a small amount of brown block crystals were obtained (yield: 8%, based on $Al(O^iPr)_3$). Selected IR peaks (cm^{-1}): 2960 (w), 1612 (s), 1570 (s), 1443 (s), 1370 (s), 1123 (m), 983 (w), 868 (m), 778 (s), 705 (s), 669 (s), 602 (m), 505 (s).

Reaction equation of $Al_{12}Pb_4$: $12Al(O^iPr)_3 + 4Pb(NO_3)_2 + 6HBA + 28H_2O + 6IM \rightarrow [Al_{12}Pb_4(BA)_6(O^iPr)_{10}(\mu_2\text{-}OH)_2(\mu_3\text{-}O)_8(\mu_4\text{-}O)_4]^{2+}\cdot 2[NO_3]^- + 6[HIM][NO_3] + 26HO^iPr$

Supplementary Fig. 6. Crystal photograph of **$Al_{12}Pb_4$**.

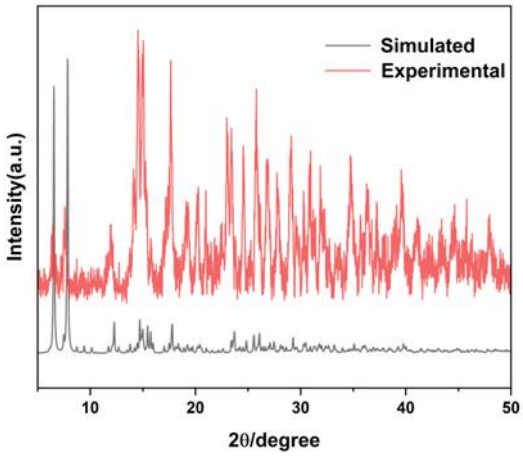

Supplementary Fig. 7. Powder X-ray diffraction (PXRD) pattern of **$Al_{12}Pb_4$**.

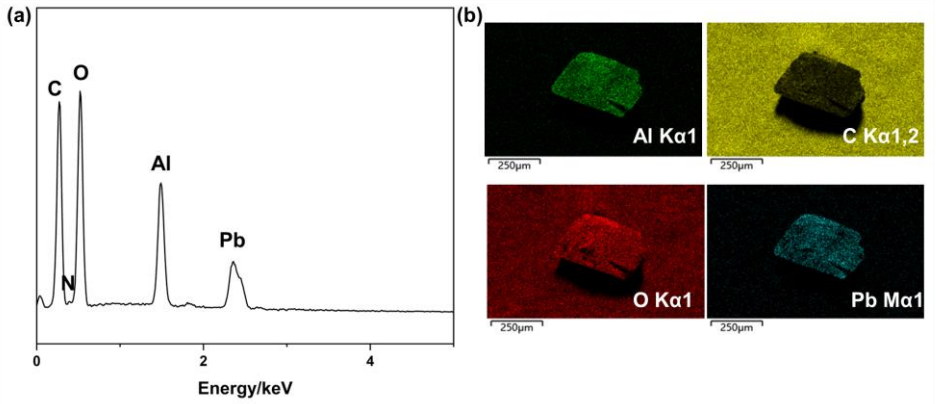

Supplementary Fig. 8. (a) Energy dispersive spectroscopy (EDS) of **$Al_{12}Pb_4$**. (b) EDS mapping of **$Al_{12}Pb_4$**.

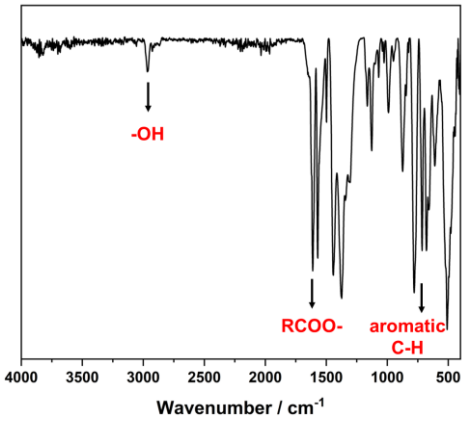

Supplementary Fig. 9. Fourier Transform Infrared (FT-IR) Spectroscopy of **$Al_{12}Pb_4$**.

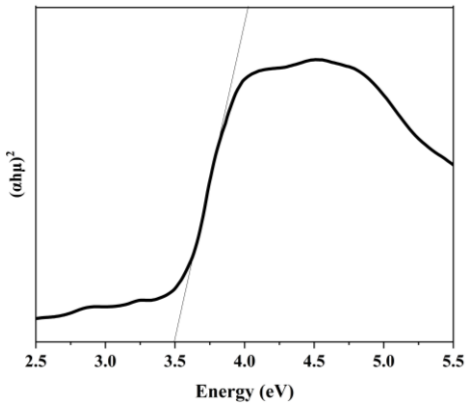

Supplementary Fig. 10. The optical bandgap of **$Al_{12}Pb_4$**.

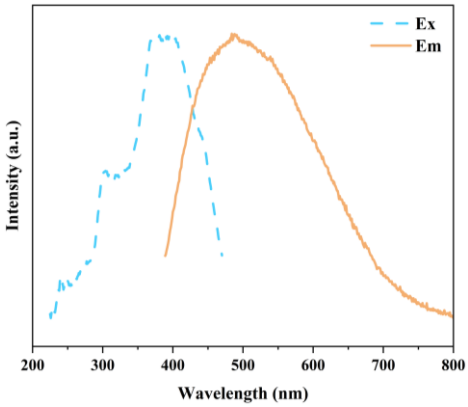

Supplementary Fig. 11. Room-temperature photoluminescence spectra of **$Al_{12}Pb_4$**.

Synthesis of $Al_{32}Pb_6L_{12}(\mu_2\text{-}O^iPr)_{20}(\mu_2\text{-}OH)_8(\mu_3\text{-}O)_{28}(\mu_4\text{-}O)_4(\mu_5\text{-}O)_2$ (L = probenecid). $Al(O^iPr)_3$ (0.204 g, 1 mmol), probenecid (0.1 g, 0.35 mmol), $Pb(NO_3)_2$ (0.1 g, 0.3 mmol), imidazole (0.068 g, 1 mmol), HO^iPr (4 mL) and DMF (1 ml) were added to a 20 mL sealed glass vial and placed in a preheated oven at 100 °C for at least 7 days. After cooling to room temperature, the bottle cap was slightly loosened to allow the solvent to evaporate slowly. After at least one week, a small amount of brown block crystals were obtained (yield: 1%, based on probenecid). Selected IR peaks (cm^{-1}): 3371 (s), 2967 (m), 2934 (m), 2873 (m), 1642 (m), 1592 (m), 1548 (m), 1382 (s), 1327 (s), 1151 (s), 1084 (m), 995 (m), 1084 (m), 863 (s), 598 (s).

Reaction equation of SAIOC-1: $32Al(O^iPr)_3 + 6Pb(NO_3)_2 + 12HL + 42H_2O + 12IM \rightarrow Al_{32}Pb_6L_{12}(\mu_2\text{-}O^iPr)_{20}(\mu_2\text{-}OH)_8(\mu_3\text{-}O)_{28}(\mu_4\text{-}O)_4(\mu_5\text{-}O)_2 + 12[HIM][NO_3] + 76HO^iPr$

Tips: The addition of tetrabutylammonium salts (~100 mg) can improve the repeatability of the reaction to a certain extent, but it is not necessary. Available tetrabutylammonium salts include tetrabutylammonium nitrate, tetrabutylammonium perchlorate, tetrabutylammonium triflate, tetrabutylammonium tetrafluoroborate and tetrabutylammonium bis((trifluoromethyl)sulfonyl)amide etc. These different anions will not affect the neutral product. The solvent evaporation process should be carried out at 10-15°C as much as possible, because too high a temperature will easily cause the solution to turn into a gel, while at too low a temperature the evaporation will be too slow and crystals will be difficult to precipitate. If the volatilization process can be continued for more than one month, there is a certain probability of obtaining several crystals of a size suitable for single crystal research.

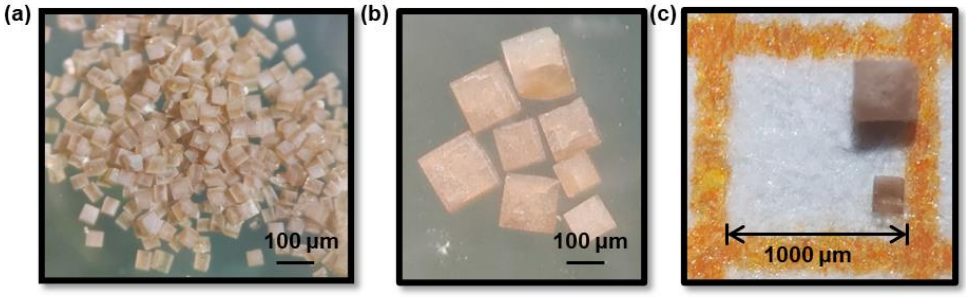

Supplementary Fig. 12. (a) Photo of ordinary crystals of **SAlOC-1**. (b) Photo of high-quality crystals of **SAlOC-1** obtained after long-term volatilization. (c) Size comparison of ordinary crystals and high-quality crystals of **SAlOC-1**.

Characterization of SAlOC-1. The difficulty in crystallization of **SAlOC-1** may be due to the large number of flexible alkyl chains on the peripheral ligands. The yield of **SAlOC-1** is low, so in the main text we focus on its single-crystal-to-single-crystal behavior. However, we still tried our best to remove impurities and picked out some pure samples for characterization. The phase purity of the compound was confirmed by PXRD (**Supplementary Fig. 13**). The elements and functional groups present in the compound were also confirmed by EDS (**Supplementary Fig. 14**) and FT-IR (**Supplementary Fig. 15**) spectroscopy, respectively. The calculated band gap for **SAlOC-1** is 3.17 eV (**Supplementary Fig. 17**), which is lower than many aluminum-oxo clusters. In addition, photoluminescence close to white light (0.31, 0.35) was observed from **SAlOC-1** with a quantum yield of 1.62% (**Supplementary Fig. 18**). These results indicate that the introduction of Pb(II) and the metal-ligand interaction can effectively affect the optical absorption and emission behaviors of the Al_{32} sphere.

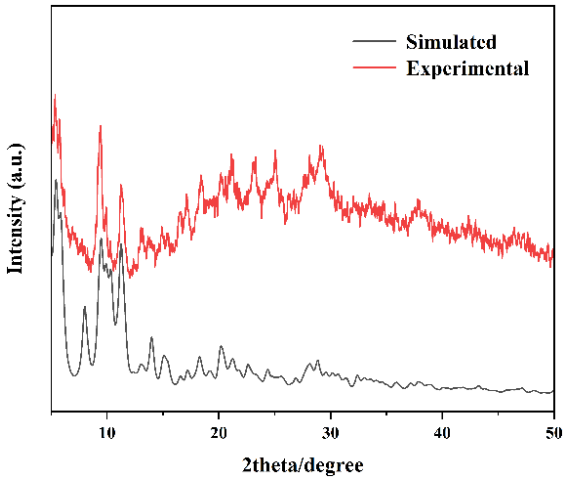

Supplementary Fig. 13. Powder X-ray diffraction (PXRD) pattern of **SAlOC-1**.

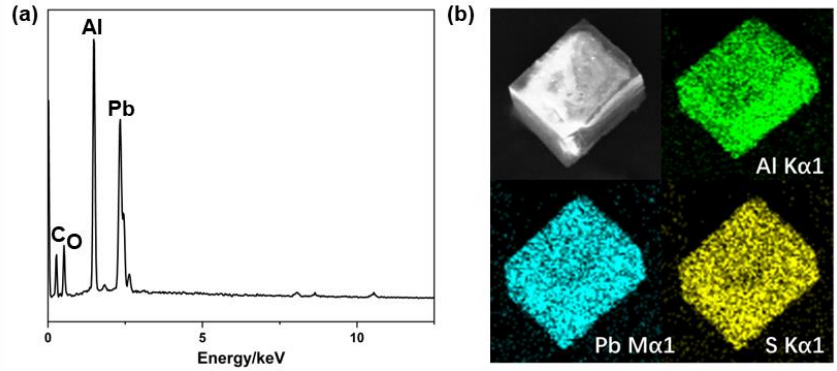

Supplementary Fig. 14. (a) Energy dispersive spectroscopy (EDS) of **SAlOC-1**. (b) EDS mapping of **SAlOC-1**.

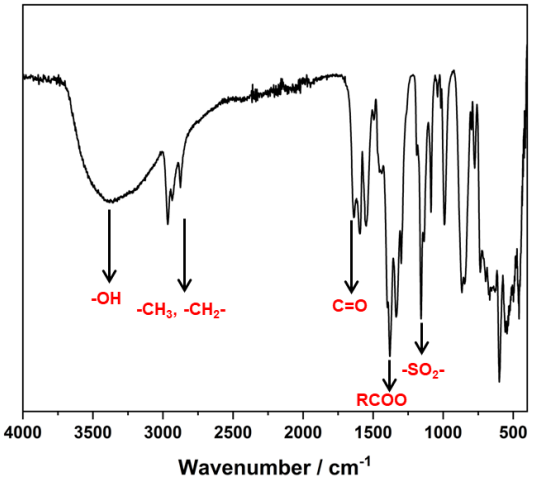

Supplementary Fig. 15. Fourier Transform Infrared (FT-IR) Spectroscopy of **SAlOC-1**.

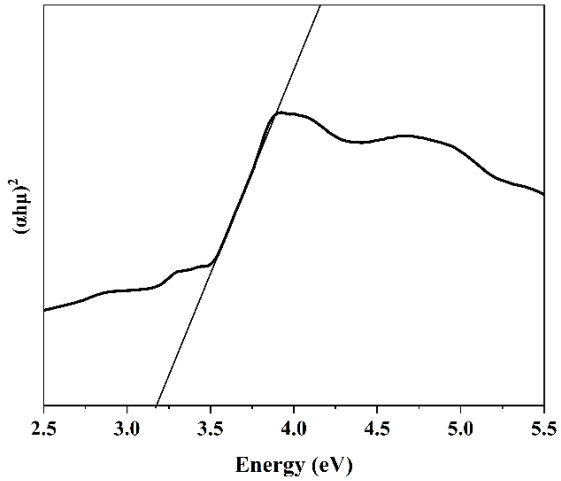

Supplementary Fig. 16. The optical bandgap of **SAlOC-1**.

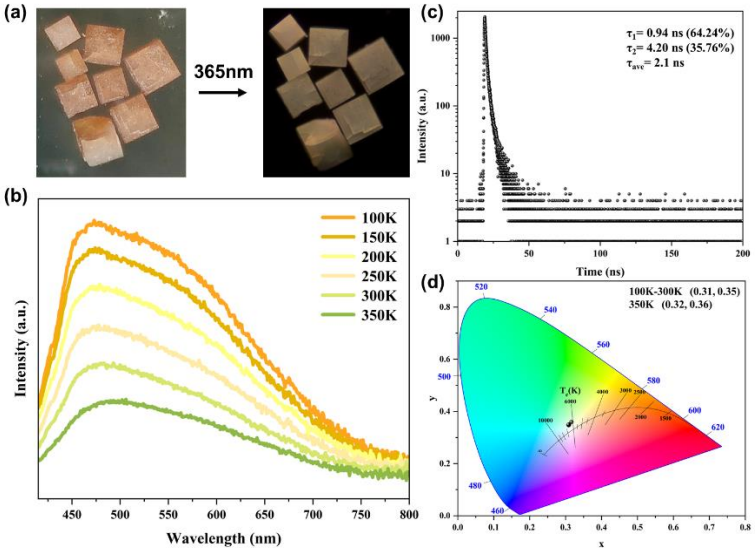

Supplementary Fig. 17. (a) Photoluminescence image of **SAlOC-1**. (b) Temperature-changing emission curve of Al_{32}. (c) Fluorescence lifetime of **SAlOC-1**. (d) Fluorescence chromaticity diagram of **SAlOC-1**.

3. Detailed Structure Information.

3.1 Molecular structure of $Al_{12}Pb_2$.

$Al_{12}Pb_2$ crystallizes in the *C*2/c space group. It helps us understand the bonding mode of the two metals because the metals are only bridged by isopropanol or oxygen atoms, and the carboxylic acid ligands do not participate in the coordination. **$Al_{12}Pb_2$** can be regarded as a dimeric structure with the Al_4Pb unit as the core, which is based on the combination of two types of Al_3O_3 fragments through edge sharing. The Pb^{2+} ion is connected to four Al3+ claws through μ_2-O^{i}Pr and is firmly anchored in the center through μ_4-O. This fragment means that when we try to obtain a closed aluminum oxo cluster, The Pb^{2+} ion may be located at its periphery, acting as a structural director with its large radius and stereochemically active lone electron pair. The side view of **$Al_{12}Pb_2$** is wavy because the Al4Pb unit is arched. If these arched units can be enclosed, it is possible to obtain a spherical structure. Another point worth noting is that the aluminum ions in the Al_4Pb unit tend to adopt four or five coordinations rather than the most common six coordinations. The lower coordination number may be conducive to the formation of a hollow spherical structure.

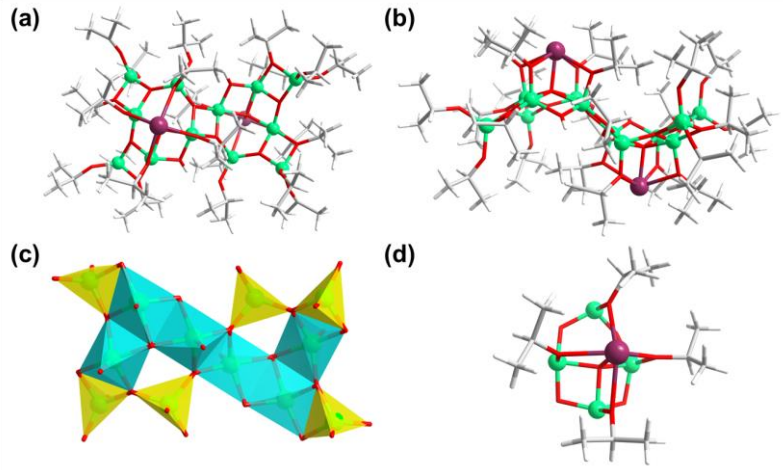

Supplementary Fig. 18. Molecular structure of **$Al_{12}Pb_2$**. (a) Top view. (b) Side view. Color code: Pb: purple, Al: green, O: red, C: grey, H: white. (c) Coordination environments of Al^{3+} ions in **$Al_{12}Pb_2$**. Color code: tetracoordinated aluminum: yellow; pentacoordinate: blue; hexacoordinated: green. (d) The arched Al_4Pb unit in **$Al_{12}Pb_2$**.

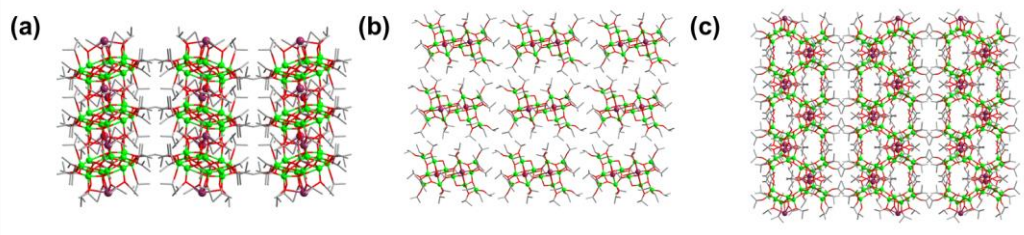

Supplementary Fig. 19. Packing diagrams of **$Al_{12}Pb_2$** in the view of (a) a-axis, (b) b-axis and (c) c-axis. Colour code: Pb: purple, Al: green, O: red, C: grey.

3.2 Molecular structure of $Al_{12}Pb_4$.

$Al_{12}Pb_4$ crystallizes in the *C*2/c space group. This is a -2-valent cation cluster, with two nitrate groups connected by hydrogen bonds on the periphery to balance the charge. The Al_{12} mini capsule is co-encapsulated by benzoic acid and Pb (II), and its structure can be regarded as a tetramer formed by the condensation of Al_4Pb units in a "head-to-head, tail-to-tail" manner. The introduction of carboxylic acid ligands replaced part of the isopropanol in the Al_4Pb unit and makes the curvature of this arched unit increased. Although we completed the enclosure of the structural unit and obtained a mini capsule that was approximately spherical, the strong π-π interaction between the ligands prevented the further expansion of the structure. This encouraged us to further explore using flexible steric ligands.

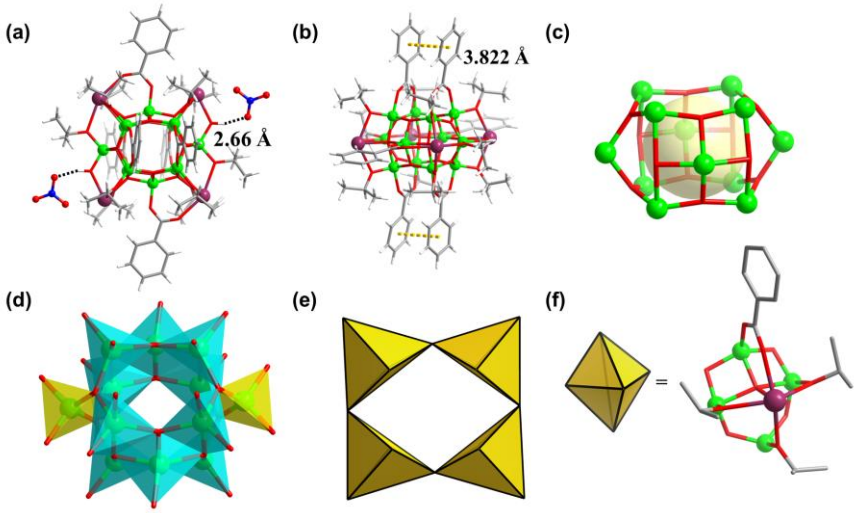

Supplementary Fig. 20. Molecular structure of **$Al_{12}Pb_4$**. (a) Top view and host-guest hydrogen bonds. (b) Side view and π-π interaction intramolecular. Color code: Pb: purple, Al: green, O: red, C: grey, H: white, N: blue. (c) Hollow mini capsule core. (d) Coordination environments of Al^{3+} ions in **$Al_{12}Pb_4$**. Color code: tetracoordinated aluminum: yellow; pentacoordinate: blue; hexacoordinated: green. (e) Schematic diagram of the Al_4Pb unit closure. (f) The Al_4Pb unit in **$Al_{12}Pb_4$**.

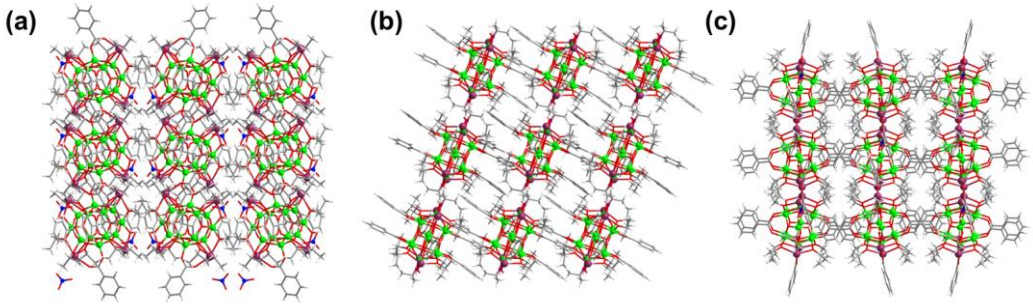

Supplementary Fig. 21. Packing diagrams of **$Al_{12}Pb_4$** in the view of (a) a-axis, (b) b-axis and (c) c-axis. Color code: Pb: purple, Al: green, O: red, C: grey, H: white, N: blue.

3.3 Molecular structure of SAlOC-1.

Core-shell structure

The alkyl chains surrounding the clusters often make structure elucidation challenging, and high-quality single crystals helped us achieve this goal. Single crystal X-ray diffraction revealed that the compound crystallized in the *P*4/n space group (No. 85). Intuitively, the overall structure of compound **SAlOC-1** can be seen as an ellipsoidal egg-shaped (molecular size: 3.1nm*3.1nm*2.5nm) core shell structure. It contains three shell including the innermost Al_{32} sphere surrounded by a "double armor" consisting of six lead atoms in the middle shell and outermost organic protect shell. The discovery of spherical Al_{32} core not only represents one of the highest nuclear aluminum oxo clusters in organic phase, but also is an unprecedented structural type in the hydrolysis chemistry of Al(III). Another point worth noting is that all aluminum atoms in the sphere are at a lower coordination number of four or five compared with the previous typical Keggin, hydrotalcite, molecular rings, Archimedes polyhedral structures dominated by six-coordinated Al(III) ions. This may also be the key factor in the formation of the unique spherical structure. Interestingly, compared to classic "truncated octahedron + cube" M_{32} clusters (O_h), the Al_{32} sphere retains the "24+8" arrangement but with a 45° twist (D_{4d},). The polyhedral twist may be attributed to the control of the organic shell and is very rare because it seems to contradict the high symmetry of the spherical structure. Importantly, lower symmetry is considered to be beneficial for host-guest chemistry studies because it reduces disorder of the guest molecules across the symmetry elements.

The six lead ions in the middle shell not only serve to confine the Al_{32} core, but also harmonize the large steric hindrance of the ligands, playing a significant role in mediating and stabilizing the structure effectively. These ions are arranged in an octahedral configuration: two are anchored at the poles via four μ_2-O^{i}Pr and one μ_5-O, while the other four are fixed at the vertices of the equatorial plane by three μ_2-O^{i}Pr, one μ_4-O, and one μ_2-COO from the ligand. All of them are pentacoordinated with tetrahedral-pyramidal geometry, influenced by stereochemically active lone pair electrons.

The outermost organic protect shell comprises twenty isopropyl alcohol groups and twelve relatively long ligands. The twenty isopropanol groups link the inner sphere to the middle shell, of which twelve are assigned to the four lead ions on the equatorial plane and the remaining eight correspond to the poles. The twelve ligands are unevenly distributed: eight on the upper hemisphere and four on the lower hemisphere. They can be categorized into three types according to their coordination environment. The first type bridges the inner sphere and the middle layer on the equatorial plane in a μ_2-(O',O'') mode (L_I). Compared to isopropanol, these ligands connect metal ions that are farther apart, resulting in weaker coordination (Pb-$O_{carboxyl}$ 2.643 Å, longer than 2.440-2.466 Å of Pb-$O_{isopropanol}$), and all oriented towards the upper hemisphere. In addition, the other eight ligands adopt a monodentate mode: four on pentacoordinated aluminum ions of the upper hemisphere (L_{II}) and four on tetracoordinated aluminum ions of the lower hemisphere (L_{III}). Their distribution is controlled by strong hydrogen bonding with μ_2-OH on the inorganic core (O-H···O 2.567-2.675 Å). This unusual mode of predominantly monodentate coordination depends not only on the raised inorganic core and intramolecular interactions, but also on the repulsive forces between ligands, and may also be affected by the

attraction of neighboring clusters (see next section). Ultimately, these three shells are interdependent and mutually influential, forming a structure that, while less symmetrical than typical spheres, achieves a high degree of harmony.

Supercluster assembly

Similar to nanoparticles, the spherical structure allows for complete exposure of surface sites. Our statistical analysis reveals that in addition to six metal sites in the central layer, there are 12 π sites, 32 hydrogen bond acceptors, and up to 120 donors provided by the probenecid ligand. L_I serves as both a hydrogen bond acceptor (sulfonyl group) and a donor (alkyl chain), binding to L_{III} of two adjacent spheres (C-H···O distances of 3.15-3.80 Å). The influence of L_{II} does not involve hydrogen bonding, but rather tetrel bonding interactions between the sulfonyl group and lead. The Pb-O distance measures 3.30 Å, approaching its bond length limit. L_{III} strongly binds to the adjacent sphere through complementary hydrogen bonds between the sulfonyl group and the aromatic ring (C-H···O distance of 3.21 Å), while also interacting with L_I of two neighboring spheres (C-H···O distances of 3.15-3.80 Å). Numerous interactions between superclusters not only impact the distribution of ligands on the sphere but crucially enable the discrete system to form highly stable configurations akin to buckles or puzzle pieces, laying a solid foundation for research in solid-state host-guest chemistry.

Because Pb occupies the inorganic core space, the number of peripheral organic protective ligands is effectively reduced, promotes the formation of pores within and between clusters. Each hemisphere of the sphere features a small cup-shaped cavity, encircled by four L_I and four L_{III} respectively, with opening widths of approximately 15.4 Å and 14.0 Å. Cavities on the sphere's sides are four irregular polyhedral spaces, bordered by surface ligands from neighboring spheres. These locations serve as ideal place for accommodating guests. Studies in host-guest chemistry indicate that guests typically favor entering these side cavities due to their increased number of supramolecular interaction sites.

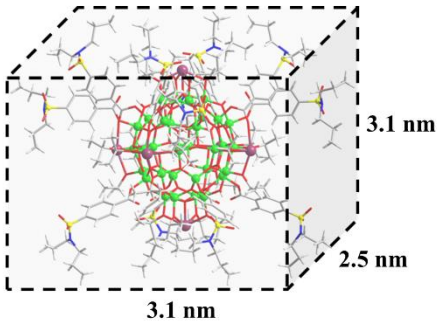

Supplementary Fig. 22. Molecular size of **SAIOC-1**.

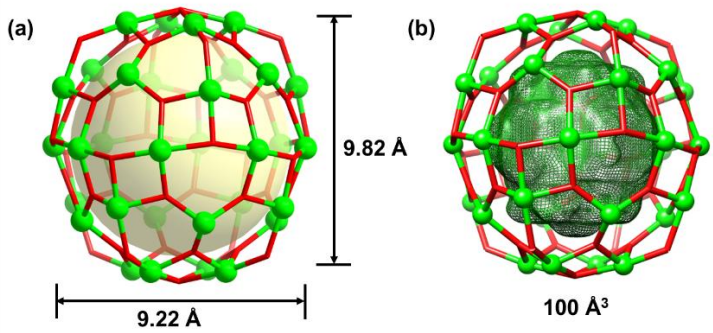

Supplementary Fig. 23. (a) Size of Al_{32} inner sphere. (b) The cavity of Al_{32} inner sphere calculated via 3V Volume Assessor program.

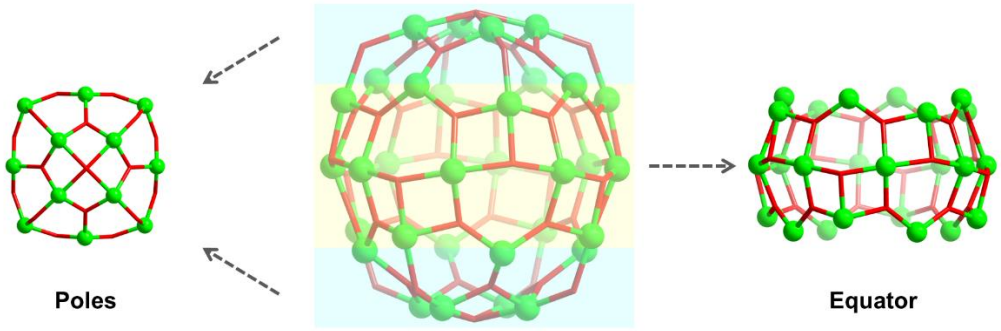

Supplementary Fig. 24. The equator and poles of Al_{32} sphere defined by different combinations of aluminum-oxo units.

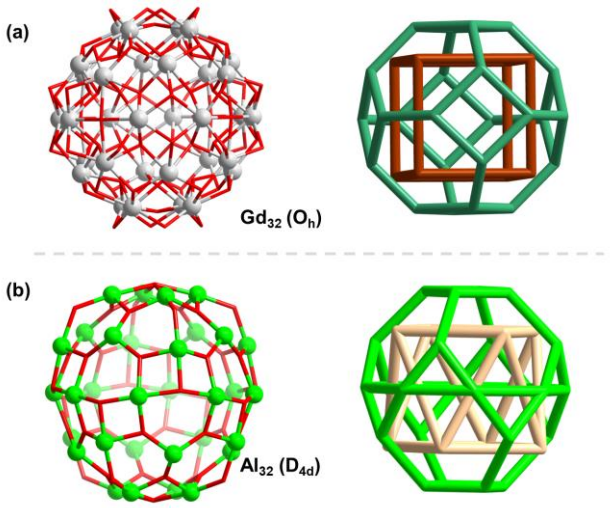

Supplementary Fig. 25. Comparison of the Al_{32} core with the classical high-symmetry 32-nuclear cluster.

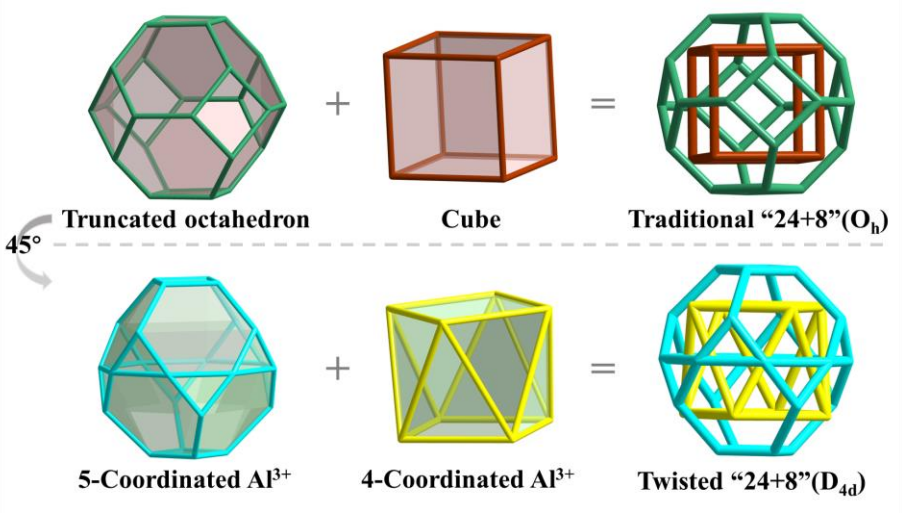

Supplementary Fig. 26. Twisted from Platonic and Archimedean polyhedra into polyhedra in Al_{32}.

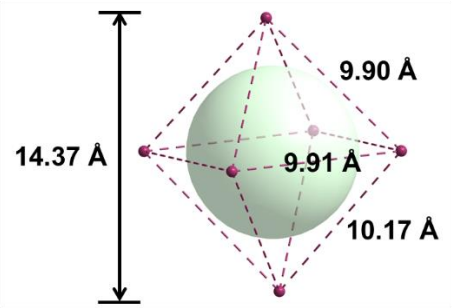

Supplementary Fig. 27. Size of the intermediate layer (Pb_6 octahedron).

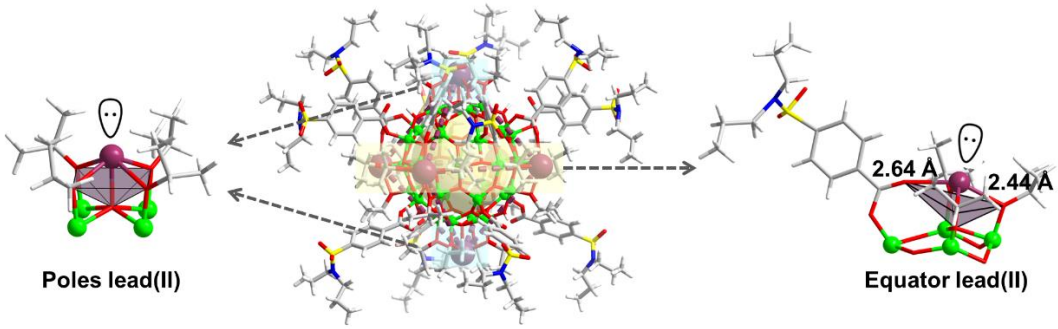

Supplementary Fig. 28. Two different coordination environments of lead ions.

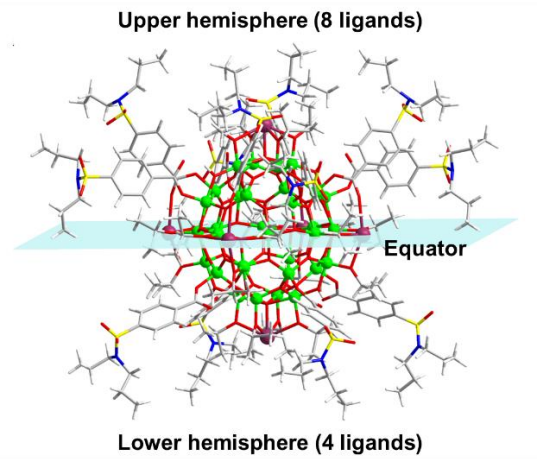

Supplementary Fig. 29. Upper and lower hemispheres defined by the number of ligands.

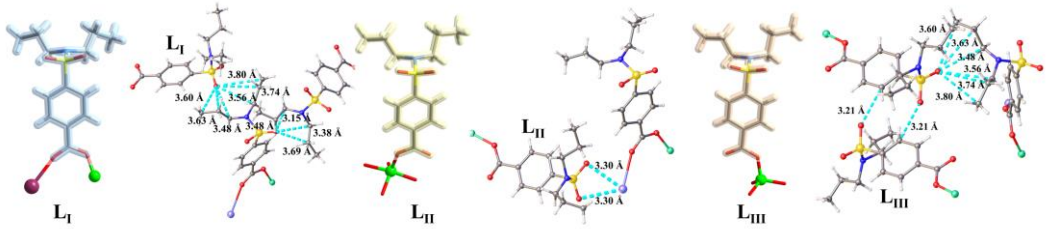

Supplementary Fig. 30. Supramolecular interactions of the organic shell of **SAIOC-1**. (L_I: bridging ligand on the upper hemisphere, L_{II}: monodentate ligand on the upper hemisphere, L_{III}: monodentate ligand on the lower hemisphere)

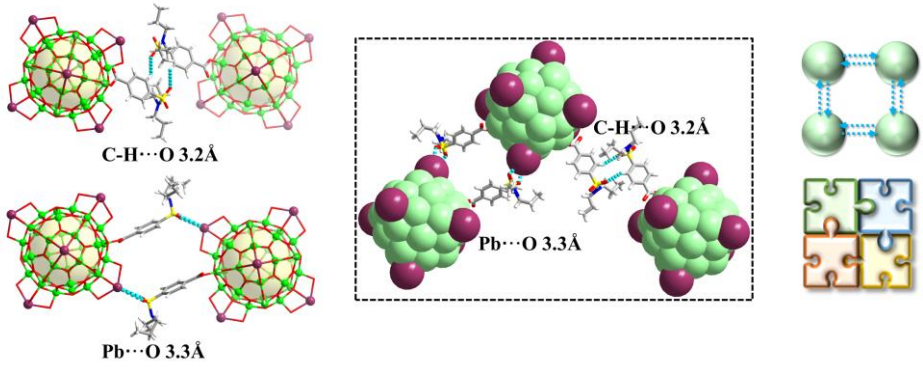

Supplementary Fig. 31. Supramolecular assembly as robust as a lock or puzzle in **SAIOC-1**.

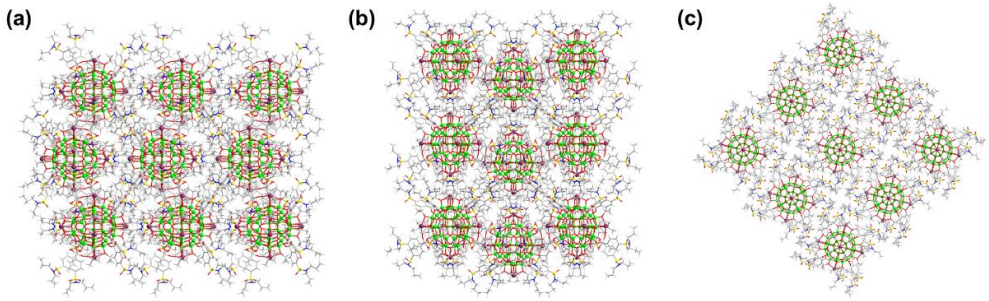

Supplementary Fig. 32. Stacking pattern of **SAIOC-1** view along (a) a-axis, (b) b-axis and (c) c-axis.

4. Supplementary information on host-guest chemistry.

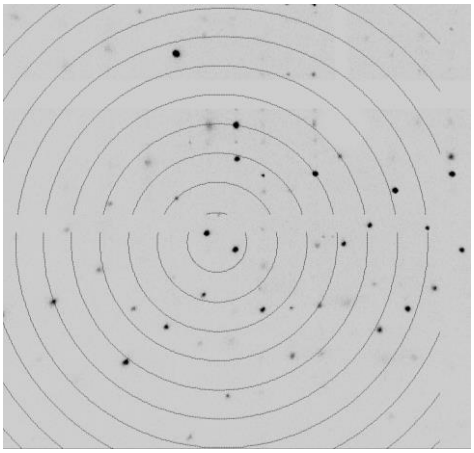

Supplementary Fig. 33. Diffraction image of a single crystal of **SAIOC-1** after being immersed in isopropanol for six months.

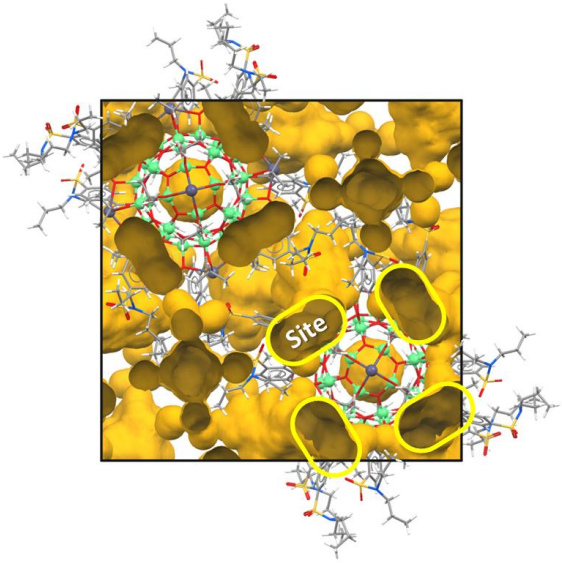

Supplementary Fig. 34. Potential guest-binding pockets in **SAIOC-1**.

4.1 Host-guest chemistry of SAIOC-1@G1.

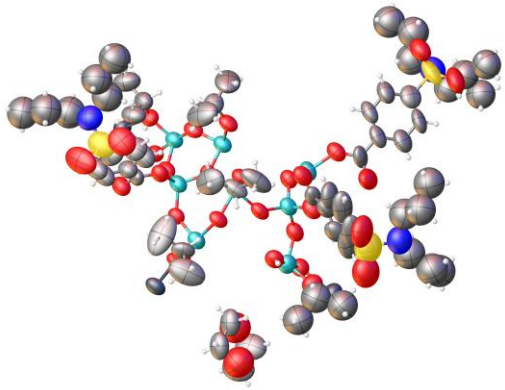

Supplementary Fig. 35. ORTEP diagrams (Thermal ellipsoids displayed at 50% probability) of the asymmetric unit of **SAIOC-1@G1**.

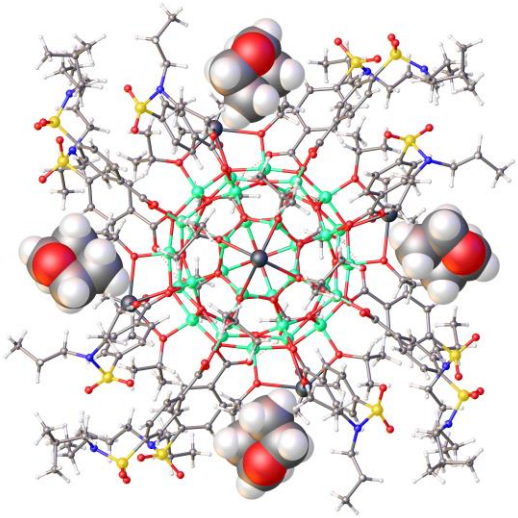

Supplementary Fig. 36. Molecular structure of **SAIOC-1@G1**.

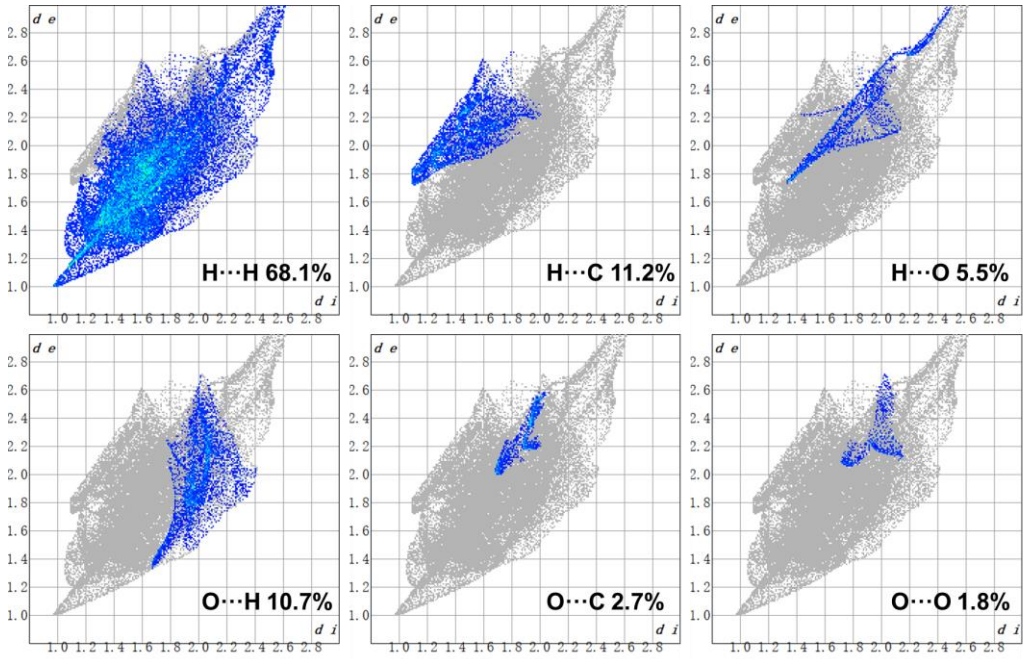

Supplementary Fig. 37. The 2D Hirschfeld fingerprint plots of **SAIOC-1@G1**.

4.2 Host-guest chemistry of SAIOC-1@G2.

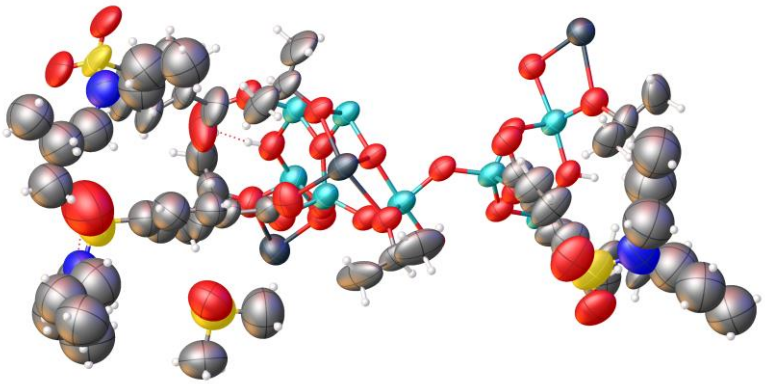

Supplementary Fig. 38. ORTEP diagrams (Thermal ellipsoids displayed at 50% probability) of the asymmetric unit of **SAIOC-1@G2**.

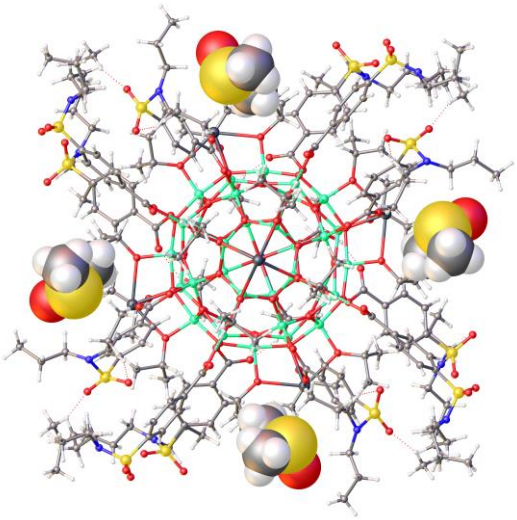

Supplementary Fig. 39. Molecular structure of **SAIOC-1@G2**.

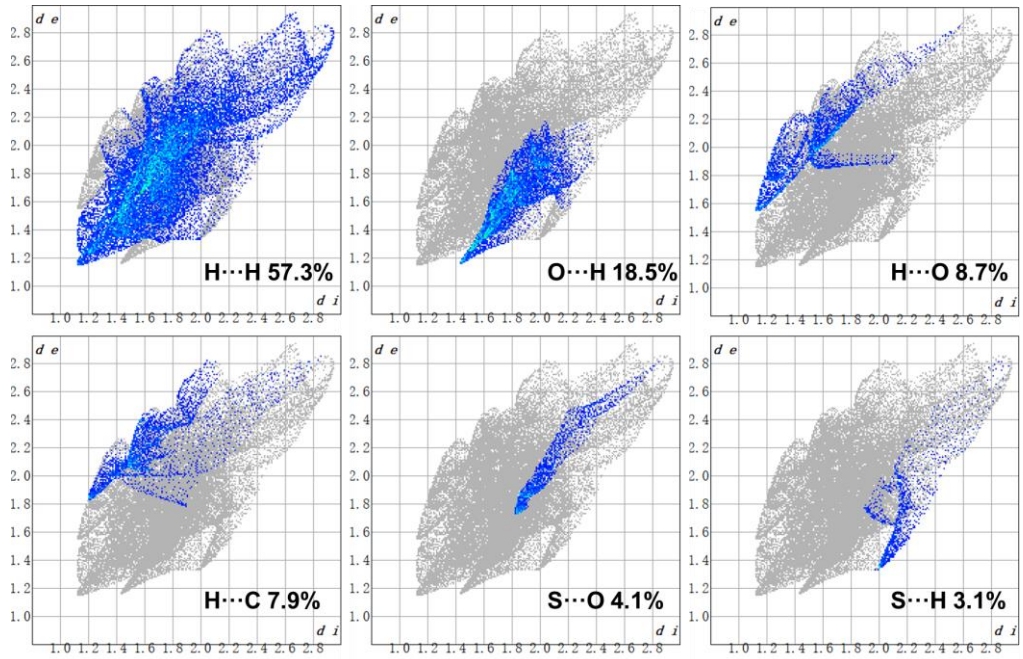

Supplementary Fig. 40. The 2D Hirschfeld fingerprint plots of **SAIOC-1@G2**.

4.3 Host-guest chemistry of SAIOC-1@G3.

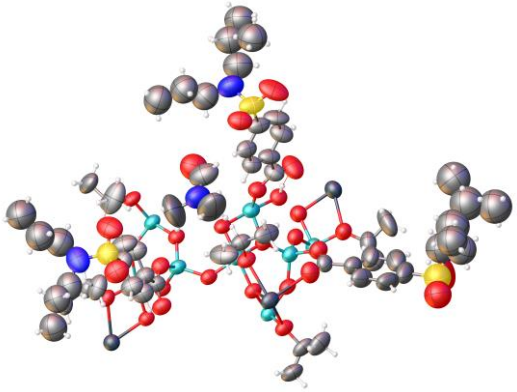

Supplementary Fig. 41. ORTEP diagrams (Thermal ellipsoids displayed at 50% probability) of the asymmetric unit of **SAIOC-1@G3**.

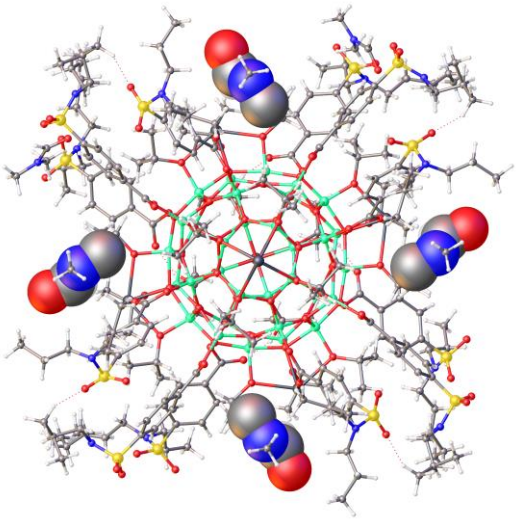

Supplementary Fig. 42. Molecular structure of **SAIOC-1@G3**.

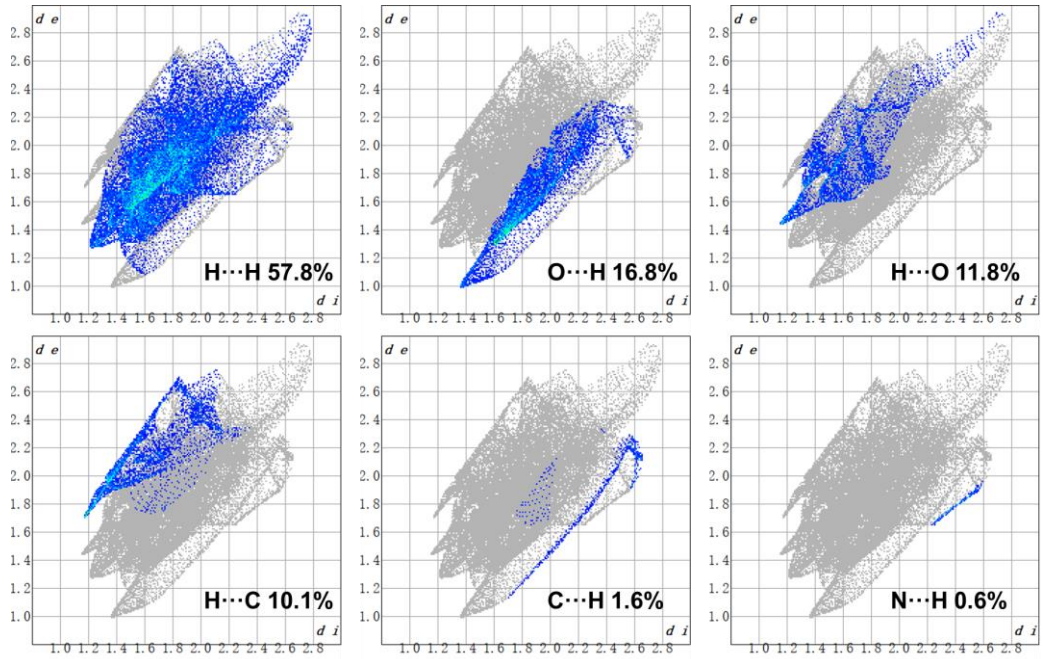

Supplementary Fig. 43. The 2D Hirschfeld fingerprint plots of **SAIOC-1@G3**.

4.4 Host-guest chemistry of SAIOC-1@G4.

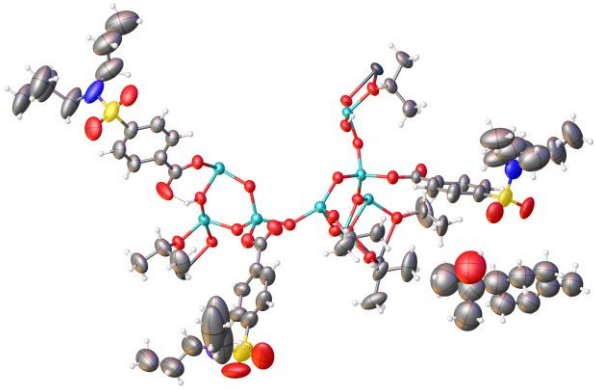

Supplementary Fig. 44. ORTEP diagrams (Thermal ellipsoids displayed at 50% probability) of the asymmetric unit of **SAIOC-1@G4**.

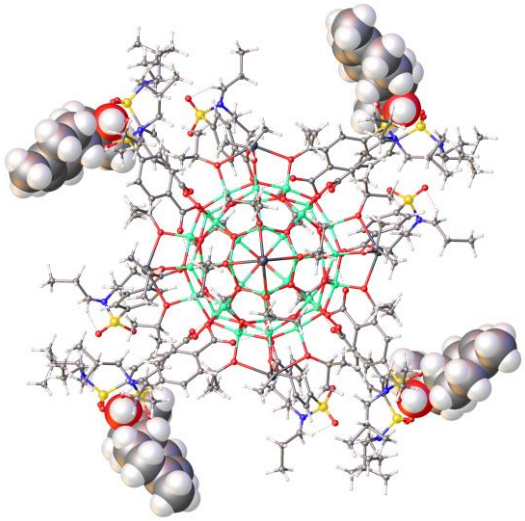

Supplementary Fig. 45. Molecular structure of **SAIOC-1@G4**.

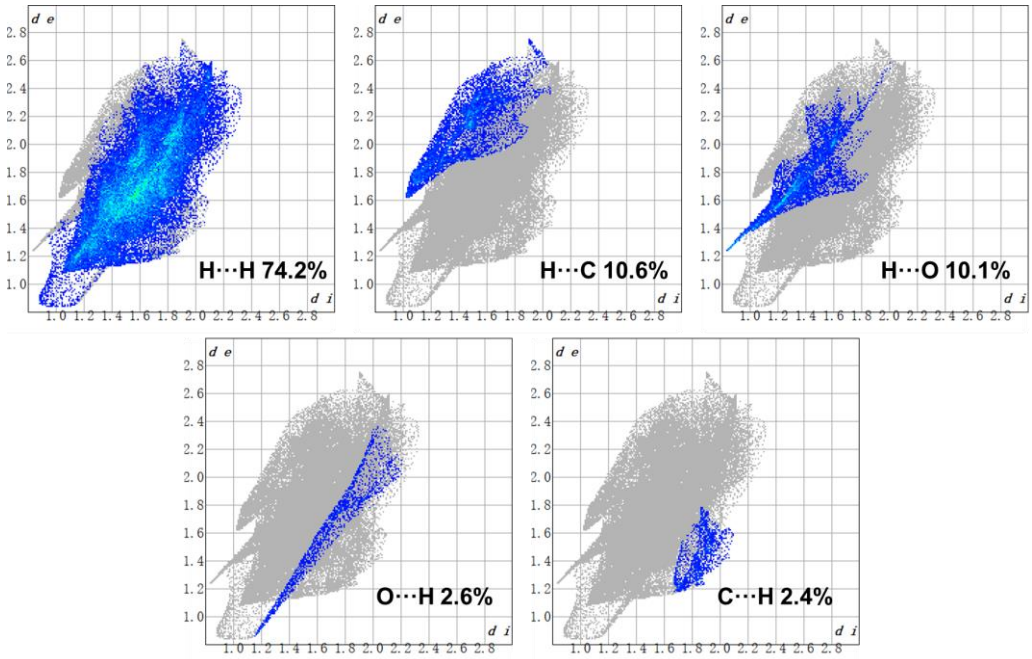

Supplementary Fig. 46. The 2D Hirschfeld fingerprint plots of **SAIOC-1@G4**.

4.5 Host-guest chemistry of SAIOC-1@G5.

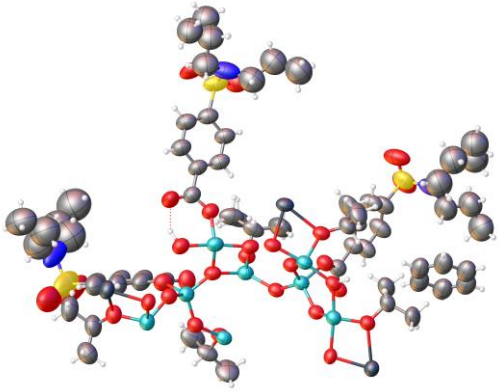

Supplementary Fig. 47. ORTEP diagrams (Thermal ellipsoids displayed at 50% probability) of the asymmetric unit of **SAIOC-1@G5**.

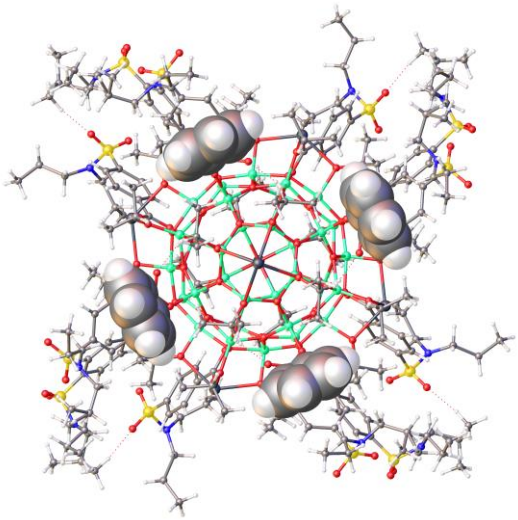

Supplementary Fig. 48. Molecular structure of **SAIOC-1@G5**.

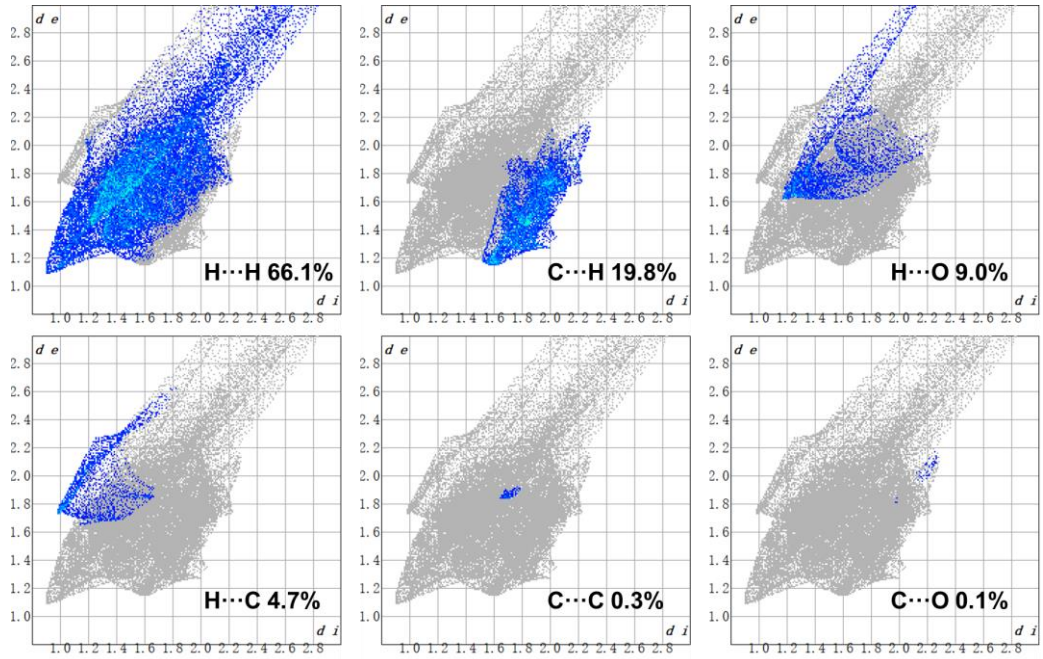

Supplementary Fig. 49. The 2D Hirschfeld fingerprint plots of **SAIOC-1@G5**.

4.6 Host-guest chemistry of SAIOC-1@G6.

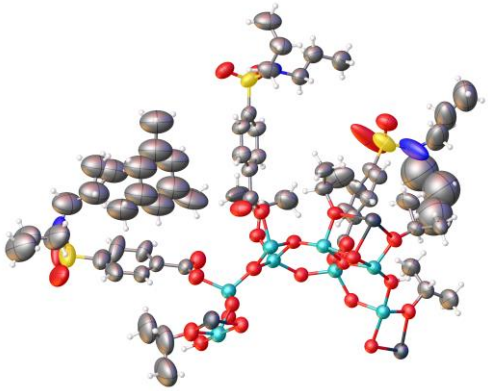

Supplementary Fig. 50. ORTEP diagrams (Thermal ellipsoids displayed at 50% probability) of the asymmetric unit of **SAIOC-1@G6**.

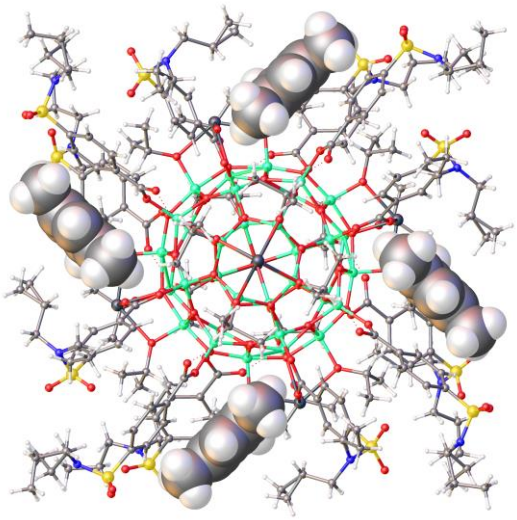

Supplementary Fig. 51. Molecular structure of **SAIOC-1@G6**.

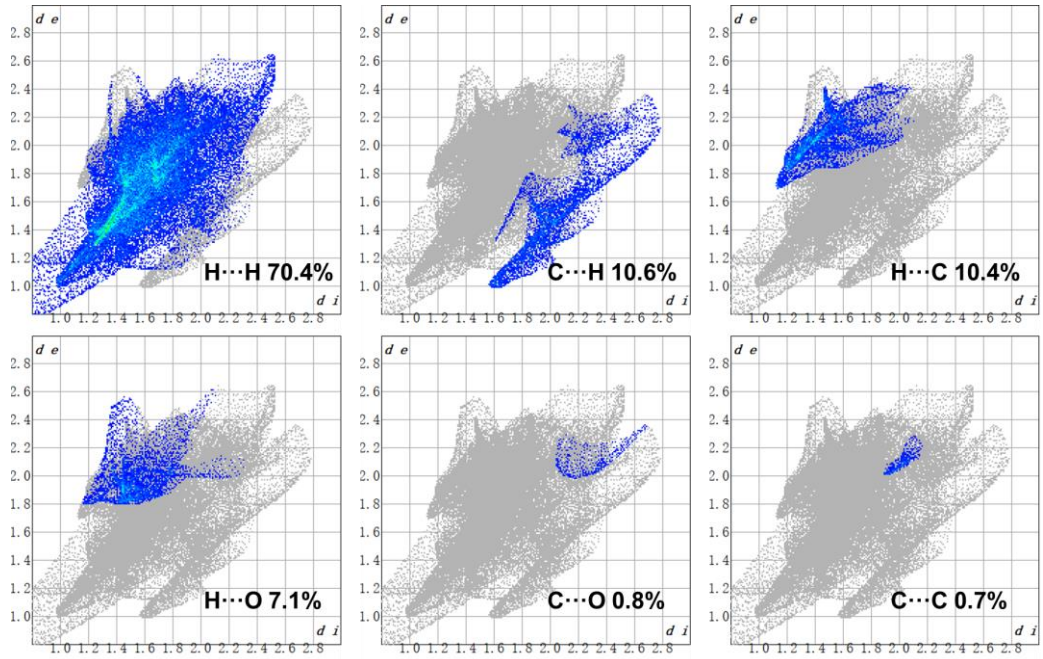

Supplementary Fig. 52. The 2D Hirschfeld fingerprint plots of **SAIOC-1@G6**.

4.7 Host-guest chemistry of SAIOC-1@G7.

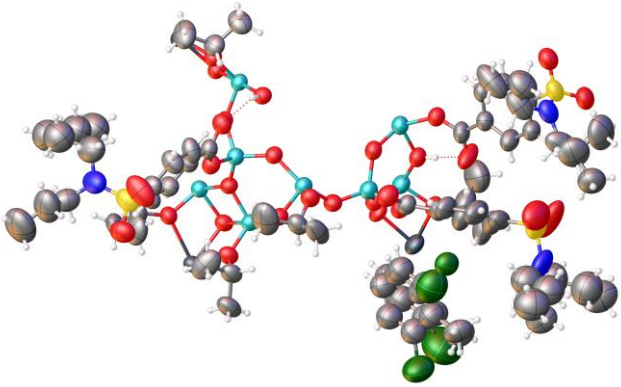

Supplementary Fig. 53. ORTEP diagrams (Thermal ellipsoids displayed at 50% probability) of the asymmetric unit of **SAIOC-1@G7**.

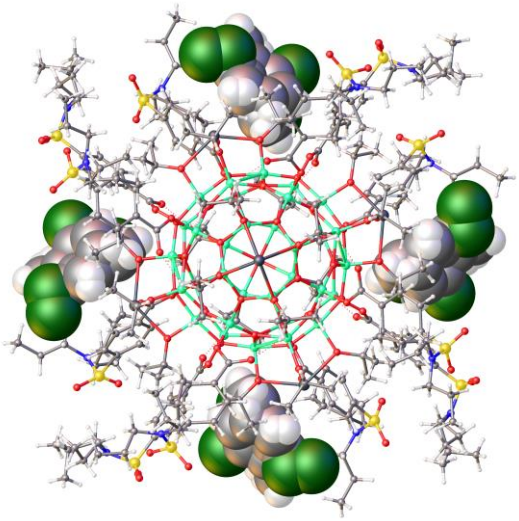

Supplementary Fig. 54. Molecular structure of **SAIOC-1@G7**.

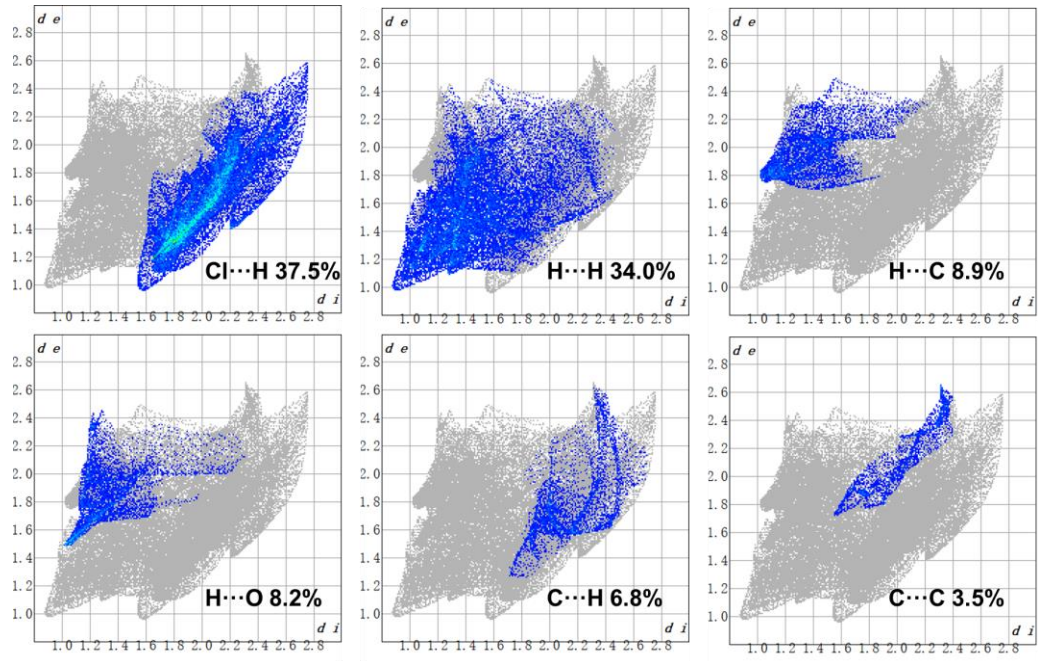

Supplementary Fig. 55. The 2D Hirschfeld fingerprint plots of **SAIOC-1@G7**.

4.8 Host-guest chemistry of SAIOC-1@G8.

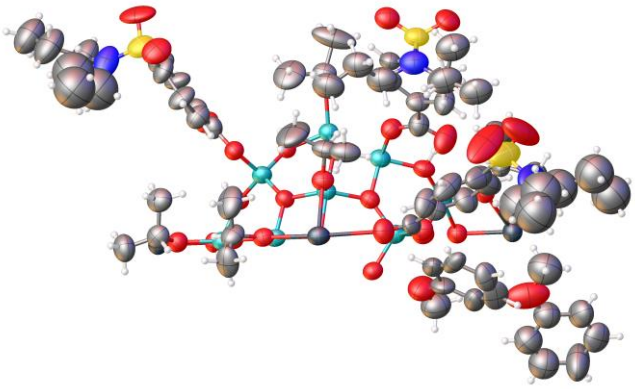

Supplementary Fig. 56. ORTEP diagrams (Thermal ellipsoids displayed at 50% probability) of the asymmetric unit of **SAIOC-1@G8**.

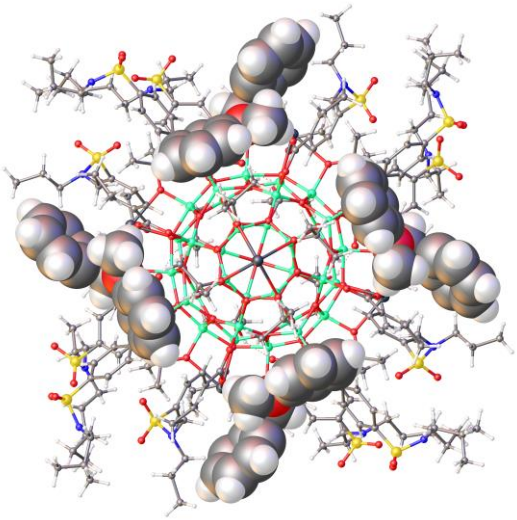

Supplementary Fig. 57. Molecular structure of **SAIOC-1@G8**.

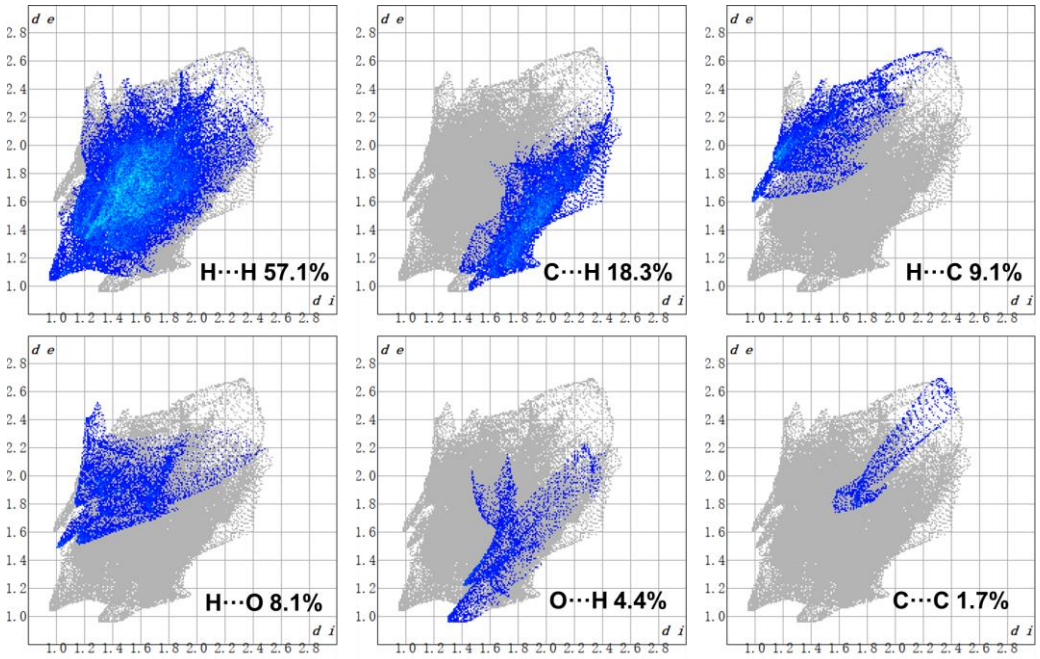

Supplementary Fig. 58. The 2D Hirschfeld fingerprint plots of **SAIOC-1@G8**.

4.9 Host-guest chemistry of SAIOC-1@G9.

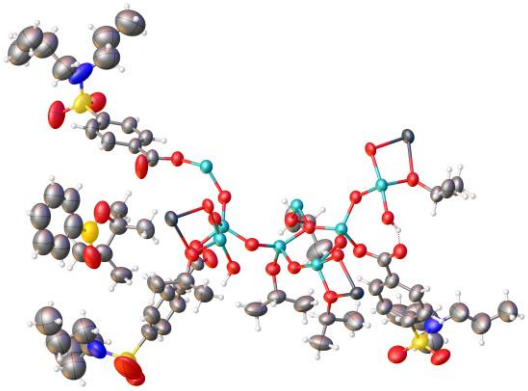

Supplementary Fig. 59. ORTEP diagrams (Thermal ellipsoids displayed at 50% probability) of the asymmetric unit of **SAIOC-1@G9**.

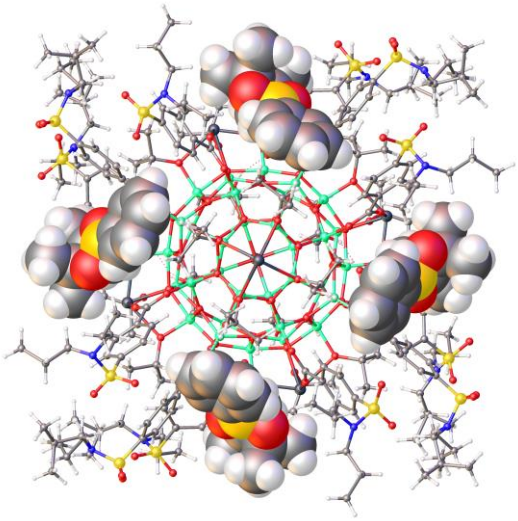

Supplementary Fig. 60. Molecular structure of **SAIOC-1@G9**.

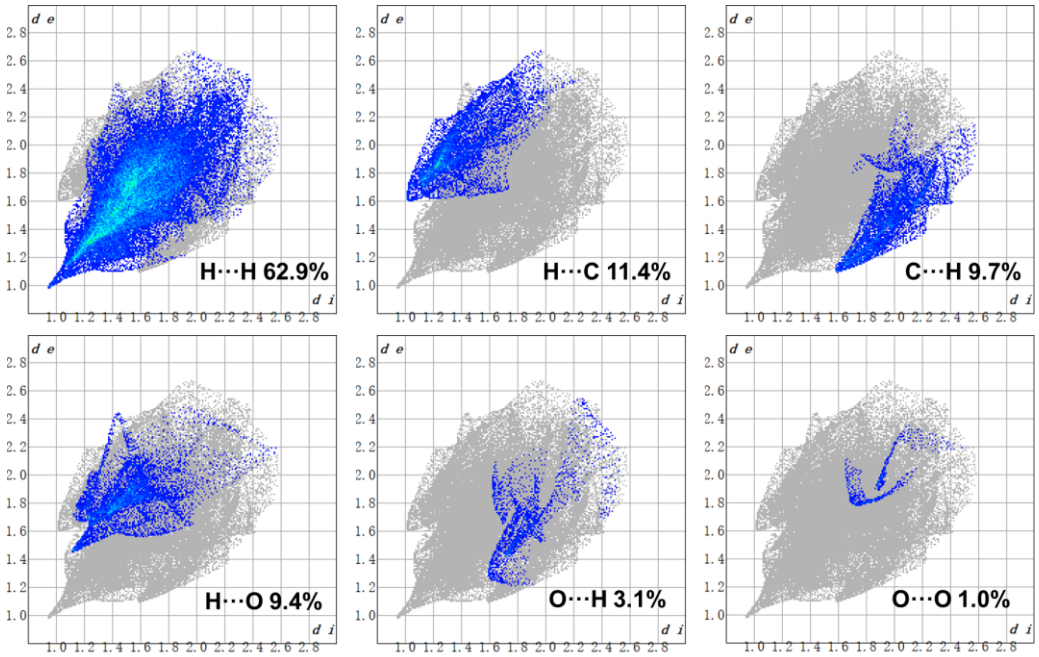

Supplementary Fig. 61. The 2D Hirschfeld fingerprint plots of **SAIOC-1@G9**.

4.10 Host-guest chemistry of SAIOC-1@G10.

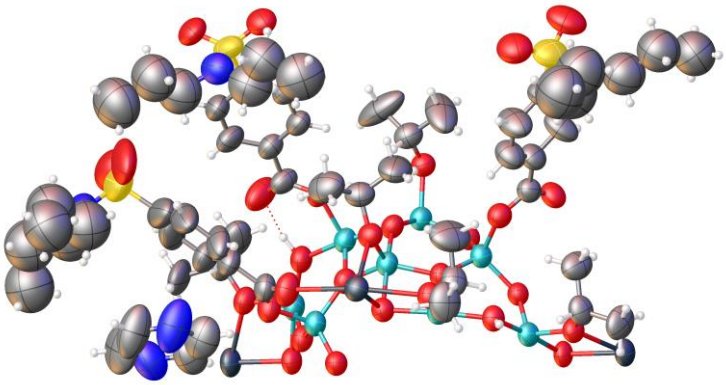

Supplementary Fig. 62. ORTEP diagrams (Thermal ellipsoids displayed at 50% probability) of the asymmetric unit of **SAIOC-1@G10**.

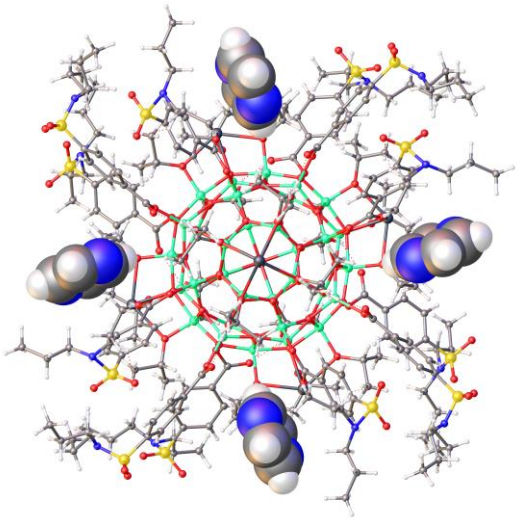

Supplementary Fig. 63. Molecular structure of **SAIOC-1@G10**.

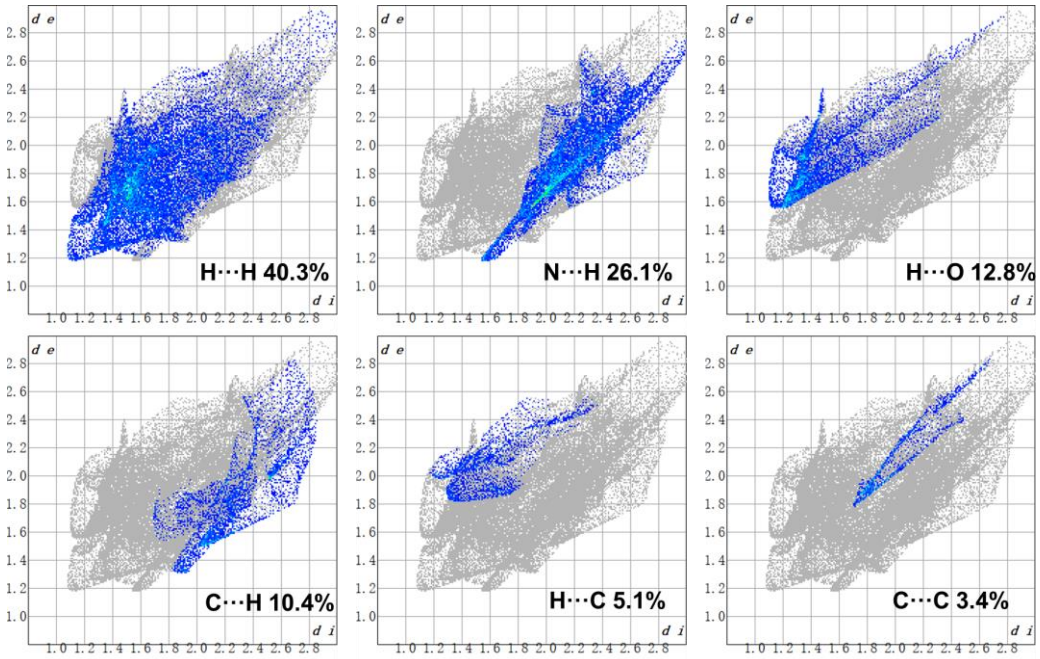

Supplementary Fig. 64. The 2D Hirschfeld fingerprint plots of **SAIOC-1@G10**.

4.11 Host-guest chemistry of SAIOC-1@G11.

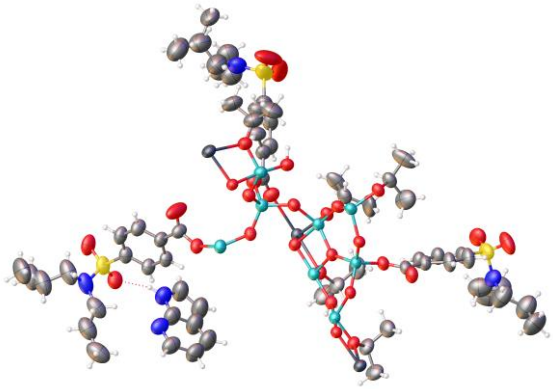

Supplementary Fig. 65. ORTEP diagrams (Thermal ellipsoids displayed at 50% probability) of the asymmetric unit of **SAIOC-1@G11**.

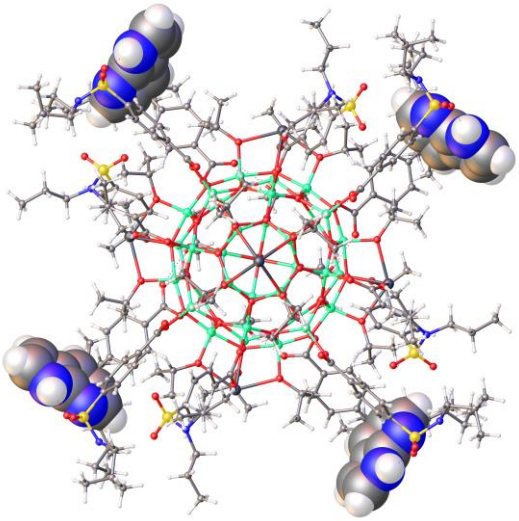

Supplementary Fig. 66. Molecular structure of **SAIOC-1@G11**.

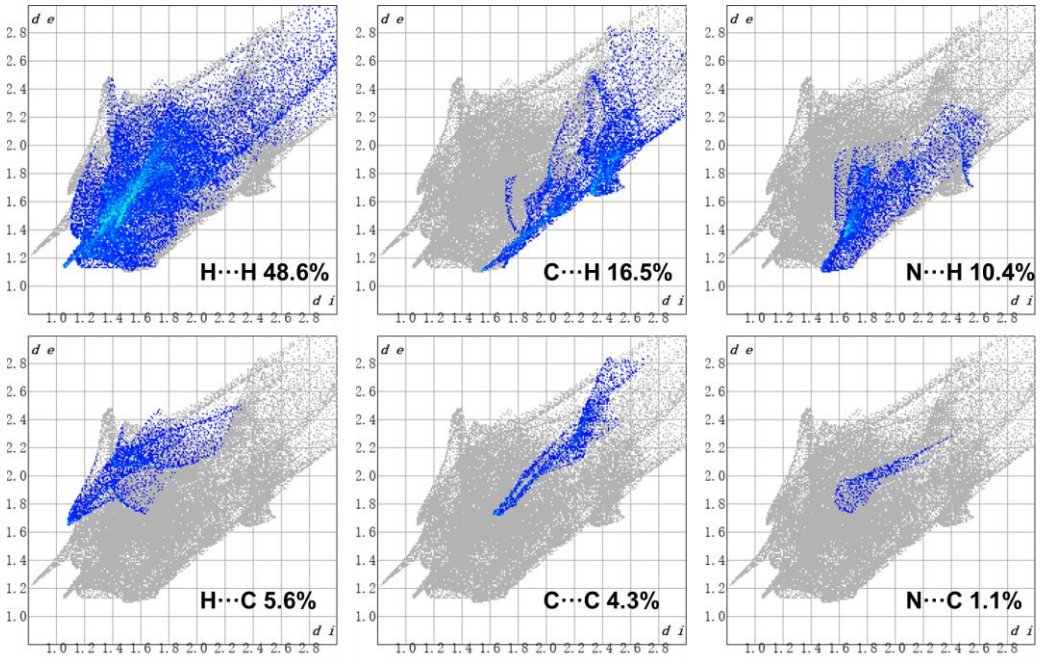

Supplementary Fig. 67. The 2D Hirschfeld fingerprint plots of **SAIOC-1@G11**.

4.12 Host-guest chemistry of SAIOC-1@G12.

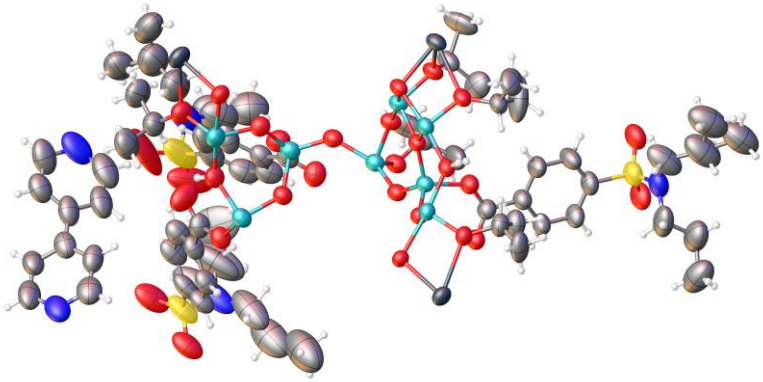

Supplementary Fig. 68. ORTEP diagrams (Thermal ellipsoids displayed at 50% probability) of the asymmetric unit of **SAIOC-1@G12**.

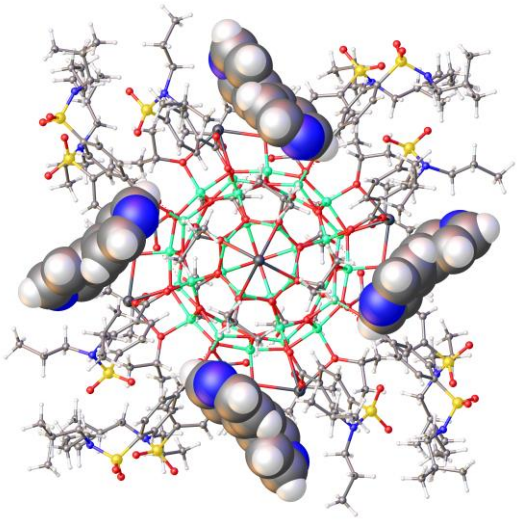

Supplementary Fig. 69. Molecular structure of **SAIOC-1@G12**.

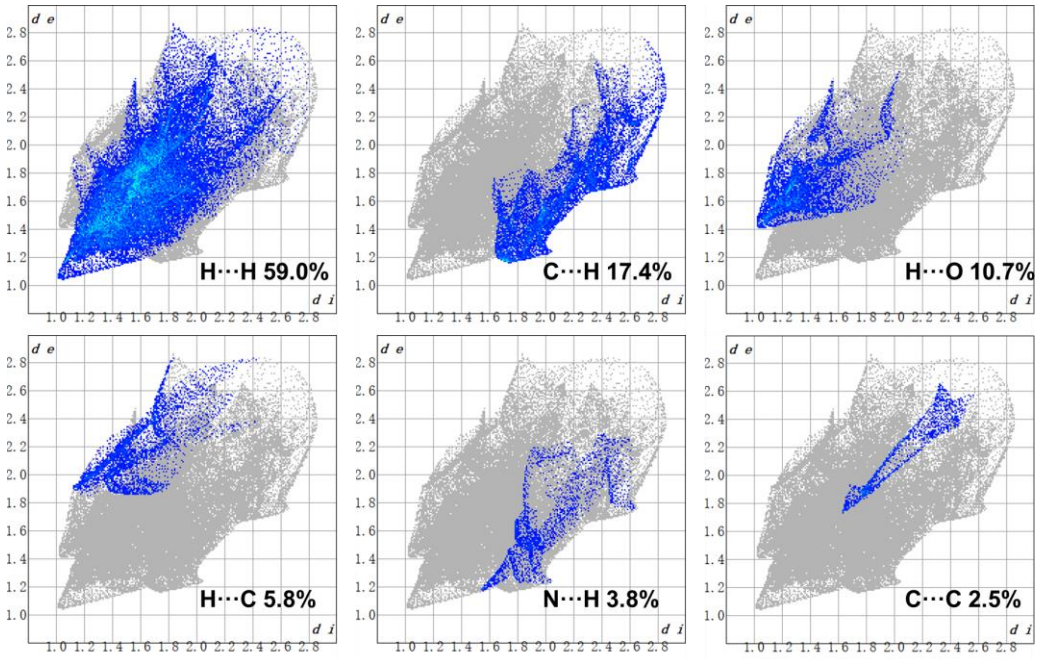

Supplementary Fig. 70. The 2D Hirschfeld fingerprint plots of **SAIOC-1@G12**.

4.13 Host-guest chemistry of SAIOC-1@G13.

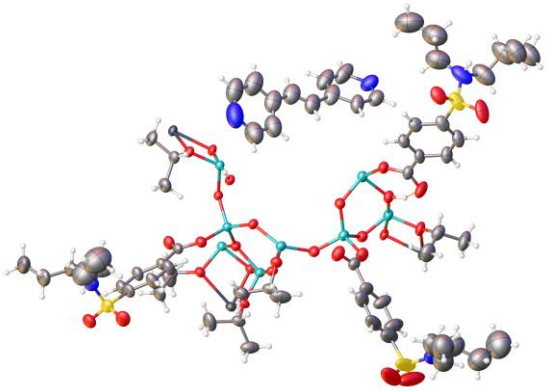

Supplementary Fig. 71. ORTEP diagrams (Thermal ellipsoids displayed at 50% probability) of the asymmetric unit of **SAIOC-1@G13**.

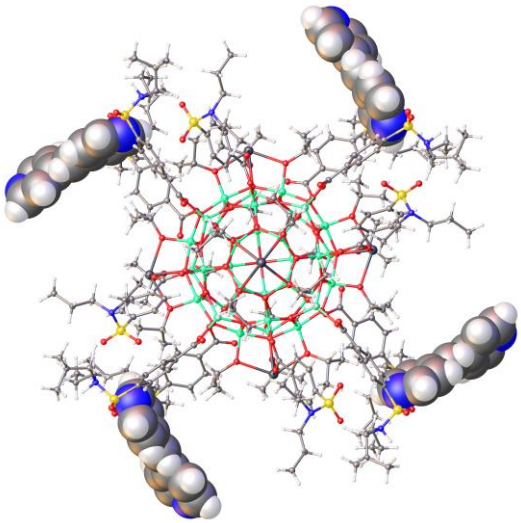

Supplementary Fig. 72. Molecular structure of **SAIOC-1@G13**.

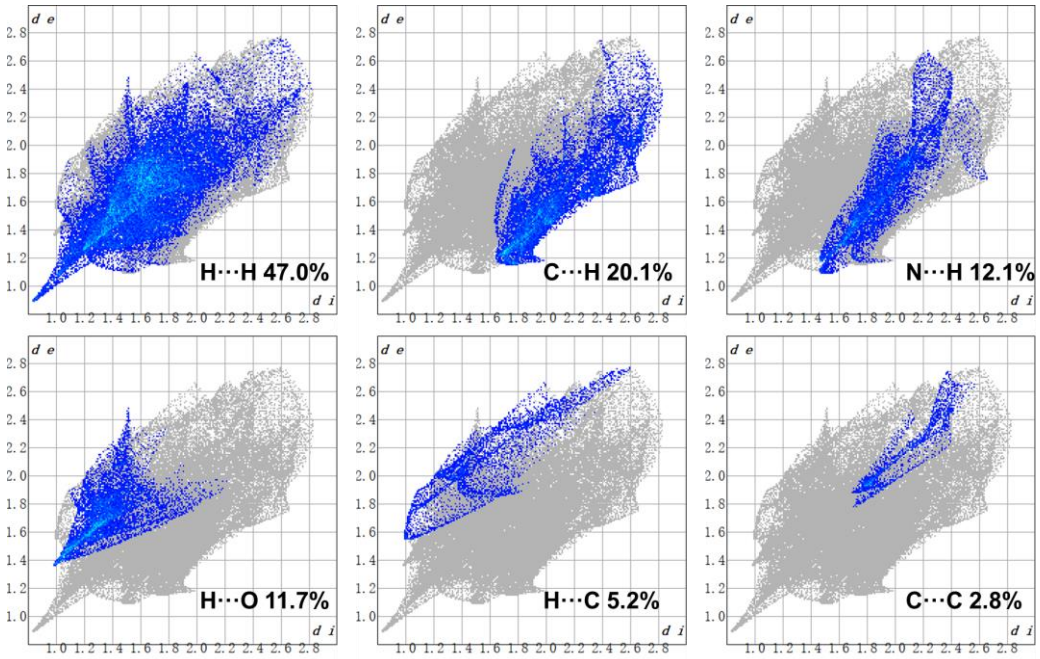

Supplementary Fig. 73. The 2D Hirschfeld fingerprint plots of **SAIOC-1@G13**.

4.14 Host-guest chemistry of SAIOC-1@G14.

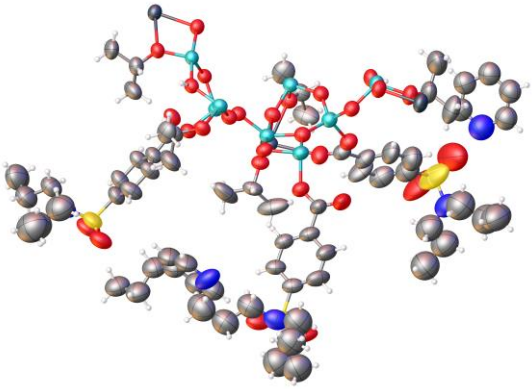

Supplementary Fig. 74. ORTEP diagrams (Thermal ellipsoids displayed at 50% probability) of the asymmetric unit of **SAIOC-1@G14**.

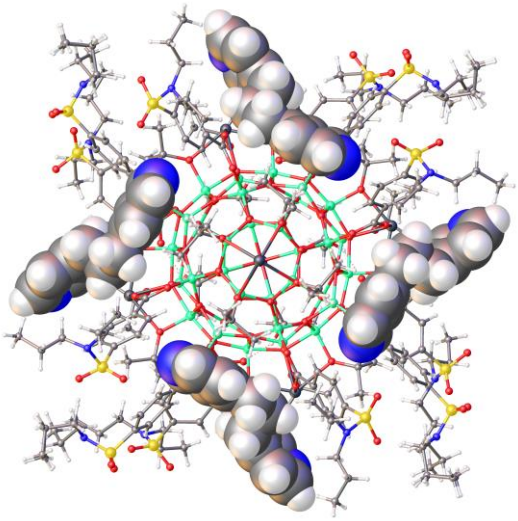

Supplementary Fig. 75. Molecular structure of **SAIOC-1@G14**.

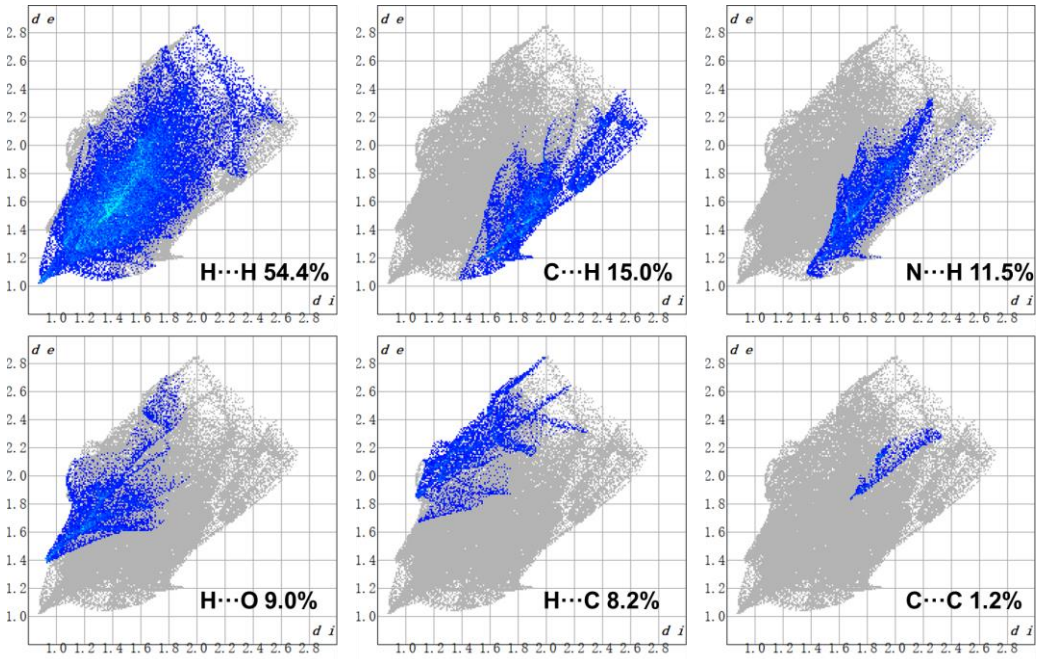

Supplementary Fig. 76. The 2D Hirschfeld fingerprint plots of **SAIOC-1@G14**.

4.15 Crystal structures of guest molecules.

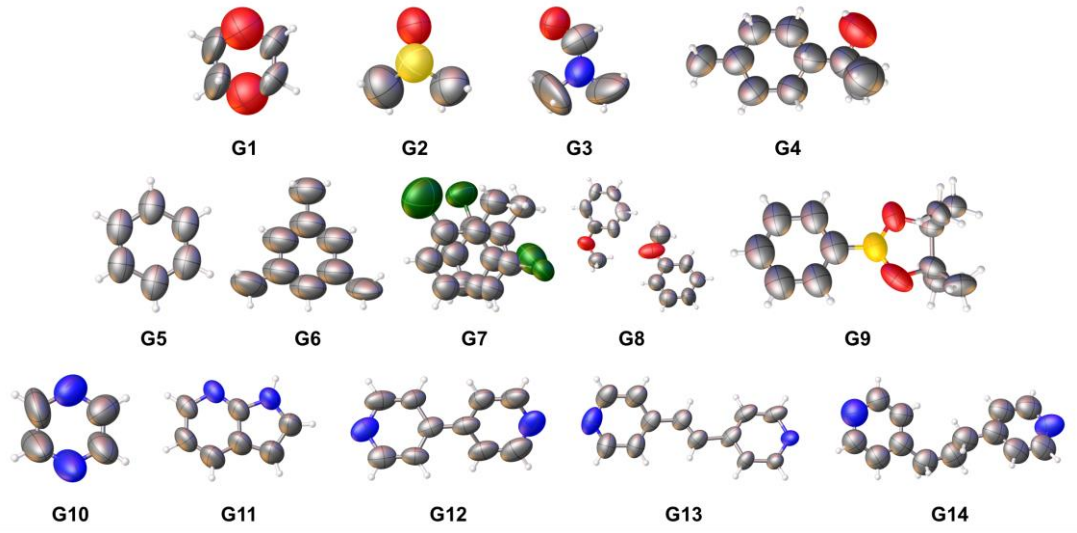

Supplementary Fig. 77. ORTEP diagrams (Thermal ellipsoids displayed at 50% probability) of guest molecules in **SAIOC-1@Guests**.

4.16 Schematic diagram of surface guest engineering.

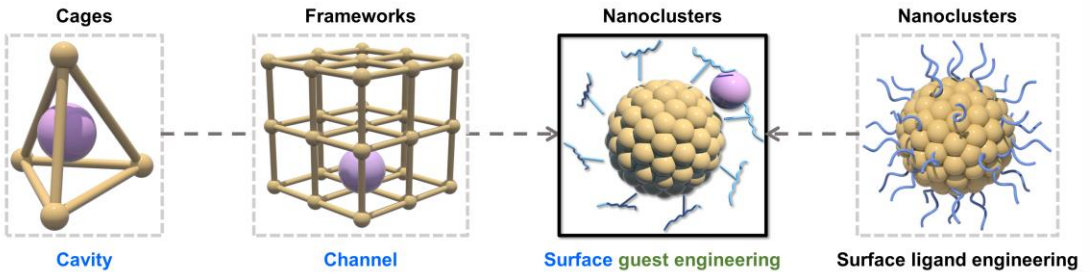

Supplementary Fig. 78. Compared with the classic framework or cage structure that relies on internal cavities or channels to accommodate guests, this work is inspired by nanoparticle surface ligand engineering and achieves the precise binding and modification of guest molecules on the surface of nanoclusters.

4.17 Selectivity of SAIOC-1 for different guests.

After immersing the crystals in a mixture of benzene and cyclohexane for 24 hours, only benzene molecules could be observed in the single crystal structure (**SAIOC-1@G5**). Considering the extremely large molecular weight of the host cluster (7380.6055), the 10 mg crystals we put in are expected to absorb only 0.25 μl of benzene (based on a host-guest ratio of 1:4, guest occupancy of 50%). This trace result can be observed to a certain extent through ^{1}H-NMR spectra, but it is difficult to further quantify.

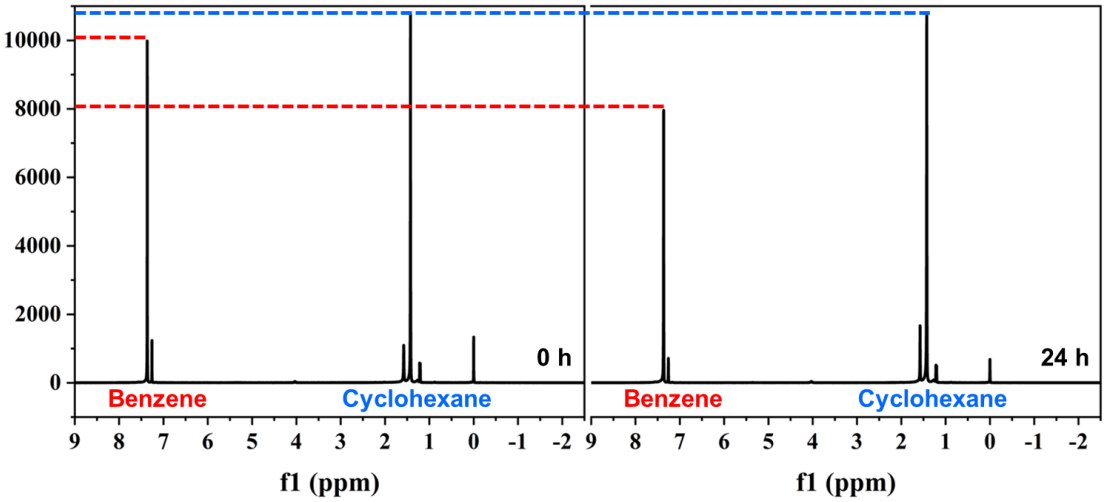

Supplementary Fig. 79. The ^{1}H-NMR spectra of a mixture of benzene and cyclohexane before and after soaking the crystals.

4.18 Guest release and recyclability of SAIOC-1.

We soaked **SAIOC-1@G10** in isopropanol for one week and then recorded it. Without the *squeeze* operation, no Q peak corresponding to the aromatic ring on the same position was observed in **SAIOC-1-recover**.

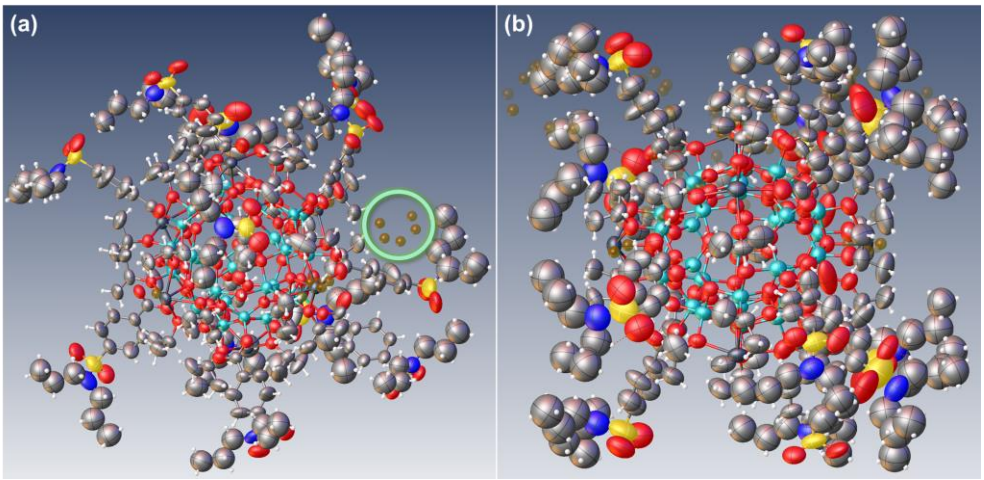

Supplementary Fig. 80. (a) Q peaks of **SAIOC-1@G10** after *squeeze* operation (the green circle is pyrazine). (b) Q peaks of **SAIOC-1-recover** before *squeeze* operation.

5. Crystallographic data, BVS analysis and hydrogen bond parameters.

Table S1. Crystallographic data and structure refinement parameters for **$Al_{12}Pb_2$, $Al_{12}Pb_4$** and **SAlOC-1**.

	$Al_{12}Pb_2$	**$Al_{12}Pb_4$**	**SAlOC-1**
Empirical formula	$C_{66}H_{154}Al_{12}O_{32}Pb_2$	$C_{72}H_{102}Al_{12}N_2O_{42}Pb_4$	$C_{216}H_{364}Al_{32}N_{12}O_{110}Pb_6S_{12}$
Formula weight	2198.02	2820.07	7380.39
Temperature / K	99.99(10)	100.00(10)	100.01(13)
Crystal system	monoclinic	monoclinic	tetragonal
Space group	*C*2/c	*C*2/c	*P*4/n
a [Å]	33.9551(3)	23.5670(2)	29.8347(2)
b [Å]	12.10050(10)	18.75520(10)	29.8347(2)
c [Å]	24.8428(3)	24.73990(10)	19.4324(3)
α [°]	90	90	90
B [°]	93.2340(10)	107.2350(10)	90
γ [°]	90	90	90
V [Å^3]	10191.00(17)	10444.12(13)	17297.0(4)
Z	4	4	2
ρ_{calcd} [g cm^{-3}]	1.433	1.793	1.417
μ [mm^{-1}]	5.455	9.355	5.261
F (000)	4504.0	5472.0	7448.0
Index ranges	–39 ≤ h ≤ 39 –14 ≤ k ≤ 14 –29 ≤ l ≤ 29	–27 ≤ h ≤ 27 –22 ≤ k ≤ 22 –22 ≤ l ≤ 29	–28 ≤ h ≤ 35 –35 ≤ k ≤ 31 –23 ≤ l ≤ 22
Reflections collected	89276	48446	198860
Independent reflections	8698 [R_{int} = 0.1144]	8884 [R_{int} = 0.0292]	15220 [R_{int} = 0.0865]
data/restraints/parameters	8698/287/527	8884/314/632	15220/429/855
Goodness-of-fit on F^2	1.048	1.027	1.042
R_1, wR_2 [$I > 2\sigma(I)$]	0.1005, 0.2457	0.0332, 0.0826	0.0667, 0.1958
R_1, wR_2 [all data]	0.1031, 0.2477	0.0341, 0.0832	0.0772, 0.2078
Largest diff. Peak/hole/e Å^{-3}	9.84/-4.21	2.98/–1.73	2.23/–0.81

Table S2. Crystallographic data and structure refinement parameters for **SAlOC-1@G1** and **SAlOC-1@G2**.

	SAlOC-1@G1	**SAlOC-1@G2**
Empirical formula	$C_{228}H_{388}Al_{32}N_{12}O_{116}Pb_6S_{12}$	$C_{222}H_{382}Al_{32}N_{12}O_{113}Pb_6S_{15}$
Formula weight	7644.70	7614.77
Temperature / K	99.97(10)	99.99(10)
Crystal system	tetragonal	tetragonal
Space group	*P*4/n	*P*4/n
a [Å]	29.9874(5)	29.8617(5)
b [Å]	29.9874(5)	29.8617(5)
c [Å]	19.1527(6)	19.1914(5)
α [°]	90	90
B [°]	90	90
γ [°]	90	90
V [Å^3]	17223.0(8)	17113.4(7)
Z	2	2
ρ_{calcd} [g cm^{-3}]	1.474	1.478
μ [mm^{-1}]	5.305	5.442
F (000)	7736.0	7700.0
	–35 ≤ h ≤ 34	–35 ≤ h ≤ 27
Index ranges	–19 ≤ k ≤ 35	–31 ≤ k ≤ 34
	–22 ≤ l ≤ 22	–12 ≤ l ≤ 22
Reflections collected	48533	54616
Independent reflections	14441 [R_{int} = 0.0745]	14557 [R_{int} = 0.0496]
data/restraints/parameters	14441/500/916	14557/512/899
Goodness-of-fit on F^2	1.047	1.042
R_1, wR_2 [$I > 2\sigma(I)$]	0.1275, 0.2844	0.0860, 0.2500
R_1, wR_2 [all data]	0.2059, 0.3416	0.1174, 0.2836
Largest diff. Peak/hole/e Å^{-3}	1.72/-0.61	1.85/-0.77

Table S3. Crystallographic data and structure refinement parameters for **SAlOC-1@G3** and **SAlOC-1@G4**.

	SAlOC-1@G3	**SAlOC-1@G4**
Empirical formula	$C_{228}H_{392}Al_{32}N_{16}O_{114}Pb_6S_{12}$	$C_{246}H_{416}Al_{32}N_{12}O_{113}Pb_6S_{12}$
Formula weight	7672.77	7841.10
Temperature / K	100.01(11)	99.97(10)
Crystal system	tetragonal	tetragonal
Space group	*P*4/n	*P*4/n
a [Å]	29.9222(4)	30.0800(2)
b [Å]	29.9222(4)	30.0800(2)
c [Å]	19.3494(4)	19.6522(2)
α [°]	90	90
B [°]	90	90
γ [°]	90	90
V [Å^3]	17324.3(6)	17781.4(3)
Z	2	2
ρ_{calcd} [g cm^{-3}]	1.471	1.465
μ [mm^{-1}]	5.275	5.144
F (000)	7768.0	7960.0
Index ranges	–34 ≤ h ≤ 35 –21 ≤ k ≤ 33 –22 ≤ l ≤ 22	–35 ≤ h ≤ 19 –33 ≤ k ≤ 18 –11 ≤ l ≤ 23
Reflections collected	51508	50077
Independent reflections	14729 [R_{int} = 0.0430]	15118 [R_{int} = 0.0367]
data/restraints/parameters	14729/281/916	15118/469/976
Goodness-of-fit on F^2	1.016	1.025
R_1, wR_2 [$I > 2\sigma(I)$]	0.0803, 0.2271	0.0481, 0.1314
R_1, wR_2 [all data]	0.1042, 0.2521	0.0557, 0.1360
Largest diff. Peak/hole/e Å^{-3}	2.72/–0.98	1.20/-0.71

Table S4. Crystallographic data and structure refinement parameters for **SAlOC-1@G5** and **SAlOC-1@G6**.

	SAlOC-1@G5	**SAlOC-1@G6**
Empirical formula	$C_{228}H_{372}Al_{32}N_{12}O_{110}Pb_6S_{12}$	$C_{243}H_{394}Al_{32}N_{12}O_{110}Pb_6S_{12}$
Formula weight	7532.57	7734.90
Temperature / K	100.01(10)	100.00(13)
Crystal system	tetragonal	tetragonal
Space group	*P*4/n	*P*4/n
a [Å]	30.0020(4)	30.0301(3)
b [Å]	30.0020(4)	30.0301(3)
c [Å]	19.4409(4)	19.2959(4)
α [°]	90	90
B [°]	90	90
γ [°]	90	90
V [Å^3]	17499.1(6)	17401.2(5)
Z	2	2
ρ_{calcd} [g cm^{-3}]	1.430	1.476
μ [mm^{-1}]	5.208	5.248
F (000)	7608.0	7832.0
Index ranges	–35 ≤ h ≤ 24 –32 ≤ k ≤ 33 –22 ≤ l ≤ 12	–32 ≤ h ≤ 34 –35 ≤ k ≤ 19 –12 ≤ l ≤ 22
Reflections collected	49850	50716
Independent reflections	14877 [R_{int} = 0.0494]	14796 [R_{int} = 0.0463]
data/restraints/parameters	14877/581/928	14796/328/934
Goodness-of-fit on F^2	1.027	1.046
R_1, wR_2 [$I > 2\sigma(I)$]	0.0785, 0.2162	0.0635, 0.1864
R_1, wR_2 [all data]	0.1013, 0.2421	0.0824, 0.2018
Largest diff. Peak/hole/e Å^{-3}	3.24/-0.67	1.95/–0.69

Table S5. Crystallographic data and structure refinement parameters for **SAIOC-1@G7** and **SAIOC-1@G8**.

	SAIOC-1@G7	**SAIOC-1@G8**
Empirical formula	$C_{244}H_{388}Al_{32}Cl_8N_{12}O_{110}Pb_6S_{12}$	$C_{251}H_{402}Al_{32}N_{12}O_{115}Pb_6S_{12}$
Formula weight	8024.46	7919.04
Temperature / K	99.99(10)	113(6)
Crystal system	tetragonal	tetragonal
Space group	*P*4/n	*P*4/n
a [Å]	30.0205(4)	30.0958(6)
b [Å]	30.0205(4)	30.0958(6)
c [Å]	19.1946(4)	19.3547(5)
α [º]	90	90
B [º]	90	90
γ [º]	90	90
V [Å^3]	17298.8(6)	17530.7(8)
Z	2	2
ρ_{calcd} [g cm^{-3}]	1.541	1.500
μ [mm^{-1}]	5.657	5.225
F (000)	8104.0	8024.0
Index ranges	–38 ≤ h ≤ 35 –24 ≤ k ≤ 36 –12 ≤ l ≤ 24	–34 ≤ h ≤ 29 –35 ≤ k ≤ 32 –22 ≤ l ≤ 12
Reflections collected	58348	48186
Independent reflections	18951 [R_{int} = 0.0535]	14853 [R_{int} = 0.0749]
data/restraints/parameters	18951/535/1042	14853/224/985
Goodness-of-fit on F^2	0.988	1.077
R_1, wR_2 [$I > 2\sigma(I)$]	0.0755, 0.2092	0.1076, 0.2726
R_1, wR_2 [all data]	0.1107, 0.2420	0.1634, 0.3415
Largest diff. Peak/hole/e Å^{-3}	2.52/-0.86	3.59/-0.99

Table S6. Crystallographic data and structure refinement parameters for **SAlOC-1@G9** and **SAlOC-1@G10**.

	SAlOC-1@G9	**SAlOC-1@G10**
Empirical formula	$C_{252}H_{413}Al_{32}B_3N_{12}O_{116}Pb_6S_{12}$	$C_{227}H_{374}Al_{32}N_{18}O_{110}Pb_6S_{12}$
Formula weight	7990.57	7606.64
Temperature / K	100.00(10)	100.00(10)
Crystal system	tetragonal	tetragonal
Space group	*P*4/n	*P*4/n
a [Å]	30.3099(3)	29.8642(5)
b [Å]	30.3099(3)	29.8642(5)
c [Å]	19.6250(3)	19.3935(4)
α [°]	90	90
B [°]	90	90
γ [°]	90	90
V [Å^3]	18029.3(5)	17296.5(7)
Z	2	2
ρ_{calcd} [g cm^{-3}]	1.472	1.461
μ [mm^{-1}]	5.085	5.276
F (000)	8104.0	7684.0
	–39 ≤ h ≤ 33	–35 ≤ h ≤ 34
Index ranges	–39 ≤ k ≤ 35	–32 ≤ k ≤ 33
	–25 ≤ l ≤ 24	–22 ≤ l ≤ 12
Reflections collected	90394	45634
Independent reflections	19912 [R_{int} = 0.0668]	14723 [R_{int} = 0.0514]
data/restraints/parameters	19912/562/1004	14723/292/897
Goodness-of-fit on F^2	1.067	1.039
R_1, wR_2 [$I > 2\sigma(I)$]	0.0664, 0.1831	0.0819, 0.2299
R_1, wR_2 [all data]	0.0898, 0.1980	0.1021, 0.2538
Largest diff. Peak/hole/e Å^{-3}	4.26/–1.45	2.46/-0.97

Table S7. Crystallographic data and structure refinement parameters for **SAlOC-1@G11** and **SAlOC-1@G12**.

	SAlOC-1@G11	**SAlOC-1@G12**
Empirical formula	$C_{237}H_{382}Al_{32}N_{18}O_{110}Pb_6S_{12}$	$C_{246}H_{384}Al_{32}N_{18}O_{110}Pb_6S_{12}$
Formula weight	7734.80	7844.91
Temperature / K	100.00(10)	100.00(10)
Crystal system	tetragonal	tetragonal
Space group	*P*4/n	*P*4/n
a [Å]	29.9251(3)	29.9771(3)
b [Å]	29.9251(3)	29.9771(3)
c [Å]	19.4257(2)	19.4854(3)
α [°]	90	90
B [°]	90	90
γ [°]	90	90
V [Å^3]	17395.9(4)	17510.1(4)
Z	2	2
ρ_{calcd} [g cm^{-3}]	1.477	1.488
μ [mm^{-1}]	5.253	5.225
F (000)	7820.0	7932.0
Index ranges	–35 ≤ h ≤ 18 –31 ≤ k ≤ 26 –12 ≤ l ≤ 22	–31 ≤ h ≤ 32 –35 ≤ k ≤ 35 –12 ≤ l ≤ 22
Reflections collected	48707	50992
Independent reflections	14763 [R_{int} = 0.0773]	14897 [R_{int} = 0.0495]
data/restraints/parameters	14763/455/949	14897/127/967
Goodness-of-fit on F^2	1.024	1.038
R_1, wR_2 [$I > 2\sigma(I)$]	0.0675, 0.1814	0.0582, 0.1554
R_1, wR_2 [all data]	0.0797, 0.1908	0.0694, 0.1635
Largest diff. Peak/hole/e Å^{-3}	2.57/-0.94	1.84/-0.71

Table S8. Crystallographic data and structure refinement parameters for **SAlOC-1@G13** and **SAlOC-1@G14**.

	SAlOC-1@G13	**SAlOC-1@G14**
Empirical formula	$C_{252}H_{398}Al_{32}N_{18}O_{110}Pb_6S_{12}$	$C_{242}H_{392}Al_{32}N_{16}O_{110}Pb_6S_{12}$
Formula weight	7931.08	7776.91
Temperature / K	100.00(14)	99.99(10)
Crystal system	tetragonal	tetragonal
Space group	*P*4/n	*P*4/n
a [Å]	29.8451(2)	30.0170(3)
b [Å]	29.8451(2)	30.0170(3)
c [Å]	19.8380(2)	19.5023(4)
α [°]	90	90
B [°]	90	90
γ [°]	90	90
V [Å^3]	17670.3(3)	17572.0(5)
Z	2	2
ρ_{calcd} [g cm^{-3}]	1.491	1.470
μ [mm^{-1}]	5.181	5.201
F (000)	8032.0	7872.0
Index ranges	–32 ≤ h ≤ 35 –23 ≤ k ≤ 35 –15 ≤ l ≤ 23	–38 ≤ h ≤ 33 –28 ≤ k ≤ 31 –22 ≤ l ≤ 25
Reflections collected	48320	58806
Independent reflections	15016 [R_{int} = 0.0534]	19373 [R_{int} = 0.0497]
data/restraints/parameters	15016/343/969	19373/436/977
Goodness-of-fit on F^2	1.028	1.047
R_1, wR_2 [$I > 2\sigma(I)$]	0.0567, 0.1522	0.0701, 0.2031
R_1, wR_2 [all data]	0.0618, 0.1562	0.0973, 0.2239
Largest diff. Peak/hole/e Å^{-3}	3.46/-1.72	2.13/-0.67

Table S9. Crystallographic data and structure refinement parameters for **SAlOC-1-revover**.

	SAlOC-1-recover
Empirical formula	$C_{216}H_{358}Al_{32}N_{12}O_{110}Pb_6S_{12}$
Formula weight	7374.34
Temperature / K	99.95(16)
Crystal system	tetragonal
Space group	*P*4/n
a [Å]	29.8435(5)
b [Å]	29.8435(5)
c [Å]	19.3447(4)
α [°]	90
B [°]	90
γ [°]	90
V [Å^3]	17229.1(7)
Z	2
ρ_{calcd} [g cm^{-3}]	1.421
μ [mm^{-1}]	5.282
F (000)	7436.0
Index ranges	–36 ≤ h ≤ 36 –23 ≤ k ≤ 38 –11 ≤ l ≤ 24
Reflections collected	51617
Independent reflections	18988 [R_{int} = 0.0475]
data/restraints/parameters	18988/744/887
Goodness-of-fit on F^2	1.003
R_1, wR_2 [$I > 2\sigma(I)$]	0.0917, 0.2668
R_1, wR_2 [all data]	0.1508, 0.3196
Largest diff. Peak/hole/e Å^{-3}	1.92/-0.66

Table S10. Selected bond lengths and bond valance summary (BVS) analysis for Al^{3+}, Pb^{2+} and μ_2-OH groups in **$Al_{12}Pb_2$**.

Atom	**Atom**	**Length/Å**	**Bond Valence**	**Atom**	**Atom**	**Length/Å**	**Bond Valence**
Al1	O2	1.807	0.65598	Al2	O2	1.844	0.59356
Al1	$O7^1$	1.913	0.49258	Al2	$O7^1$	1.898	0.51295
Al1	$O16^1$	1.847	0.58876	Al2	$O5^1$	1.798	0.67213
Al1	$O13^1$	1.839	0.60163	Al2	O5	1.787	0.69242
Al1	O1	1.758	0.74887	Al2	O4	1.772	0.72106
Al1			**3.08782**	**Al2**			**3.19213**
Atom	**Atom**	**Length/Å**	**Bond Valence**	**Atom**	**Atom**	**Length/Å**	**Bond Valence**
Al3	O5	1.756	0.75293	Al4	O8	1.79	0.68683
Al3	O8	1.763	0.73882	Al4	O11	1.813	0.64543
Al3	O3	1.742	0.78196	Al4	O9	1.672	0.94482
Al3	O6	1.776	0.71331	Al4	O10	1.684	0.91467
Al3			**2.98702**	**Al4**			**3.19175**
Atom	**Atom**	**Length/Å**	**Bond Valence**	**Atom**	**Atom**	**Length/Å**	**Bond Valence**
Al5	O7	1.913	0.49258	Al6	O16	1.837	0.60489
Al5	O8	1.832	0.61312	Al6	O13	1.763	0.73882
Al5	O12	1.779	0.70755	Al6	O15	1.705	0.8642
Al5	O13	1.795	0.67761	Al6	O14	1.683	0.91715
Al5	O11	1.888	0.52701				
Al5			**3.01786**	**Al6**			**3.12506**
Atom	**Atom**	**Length/Å**	**Bond Valence**	**Atom**	**Atom**	**Length/Å**	**Bond Valence**
Pb1	O7	2.182	0.71222	O2	Al1	1.807	0.65598
Pb1	O12	2.438	0.3991	O2	Al2	1.844	0.59356
Pb1	O6	2.553	0.30767				
Pb1	$O4^1$	2.508	0.34064				
Pb1	$O1^1$	2.544	0.314				
Pb1			**2.07363**	**O2**			**1.24954**
Symmetric code: ^{1}3/2-X,1/2-Y,1-Z							

Table S11. Selected bond lengths and bond valance summary (BVS) analysis for Al^{3+}, Pb^{2+} and μ_2-OH groups in **$Al_{12}Pb_4$**.

Atom	**Atom**	**Length/Å**	**Bond Valence**	**Atom**	**Atom**	**Length/Å**	**Bond Valence**
Al1	O18	1.781	0.70374	Al2	O18	1.78	0.70564
Al1	O12[1]	1.988	0.4022	Al2	O14	1.804	0.66132
Al1	O6	1.794	0.67944	Al2	O7[1]	1.978	0.41322
Al1	O21	1.77	0.72497	Al2	O16	1.882	0.53562
Al1	O19	1.882	0.53562	Al2	O17	1.777	0.71139
Al1			**3.04597**	**Al2**			**3.02719**
Atom	**Atom**	**Length/Å**	**Bond Valence**	**Atom**	**Atom**	**Length/Å**	**Bond Valence**
Al3	O11	1.777	0.71139	Al4	O18[1]	1.809	0.65245
Al3	O13	1.78	0.70564	Al4	O11	1.814	0.64369
Al3	O14	1.798	0.67213	Al4	O12	1.863	0.56385
Al3	O12	2.011	0.37796	Al4	O71	1.865	0.56081
Al3	O15	1.886	0.52986	Al4	O10	1.813	0.64543
Al3			**2.99698**	**Al4**			**3.06622**
Atom	**Atom**	**Length/Å**	**Bond Valence**	**Atom**	**Atom**	**Length/Å**	**Bond Valence**
Al5	O11	1.786	0.69429	Al6	O5	1.755	0.75497
Al5	O6	1.793	0.68128	Al6	O4	1.764	0.73682
Al5	O7	1.973	0.41884	Al6	O14[1]	1.767	0.73087
Al5	O20	1.88	0.53853	Al6	O6	1.772	0.72106
Al5	O8	1.772	0.72106				
Al5			**3.054**	**Al6**			**2.94373**
Atom	**Atom**	**Length/Å**	**Bond Valence**	**Atom**	**Atom**	**Length/Å**	**Bond Valence**
Pb1	O5	2.555	0.30628	Pb2	O13	2.42	0.41568
Pb1	O7	2.301	0.54411	Pb2	O4[1]	2.278	0.57318
Pb1	O17[1]	2.426	0.41008	Pb2	O12	2.258	0.59971
Pb1	O8	2.462	0.378	Pb2	O21[1]	2.46	0.37972
Pb1	O9	2.48	0.36292				
Pb1	O22	2.49	0.3548				
Pb1			**2.3562**	**Pb2**			**1.96829**
Atom	**Atom**	**Length/Å**	**Bond Valence**				
O4	Pb2	2.278	0.57318				
O4	Al6	1.764	0.73682				
O4			**1.31**				
Symmetric code: [1]1/2-X,1/2-Y,1-Z							

Table S12. Selected bond lengths and bond valance summary (BVS) analysis for Al^{3+}, Pb^{2+} and μ_2-OH groups in **SAlOC-1**.

Atom	Atom	Length/Å	Bond Valence	Atom	Atom	Length/Å	Bond Valence
Al1	O11	1.785	0.69617	Al2	O11	1.778	0.70947
Al1	O11^{2}	1.785	0.69617	Al2	O15	1.727	0.81432
Al1	O12	2.055	0.33558	Al2	O10	1.735	0.7969
Al1	O23	1.779	0.70755	Al2	O00Y	1.771	0.72302
Al1	O14	1.831	0.61478				
Al1			**3.05025**	**Al2**			**3.0437**
Atom	**Atom**	**Length/Å**	**Bond Valence**	**Atom**	**Atom**	**Length/Å**	**Bond Valence**
Al3	O8	1.833	0.61147	Al4	O22^{1}	1.837	0.60489
Al3	O9	1.875	0.54585	Al4	O16	1.926	0.47557
Al3	O15^{1}	1.792	0.68312	Al4	O9	1.822	0.62992
Al3	O10	1.807	0.65598	Al4	O10	1.832	0.61312
Al3	O14^{1}	1.853	0.57929	Al4	O17	1.788	0.69055
Al3			**3.07572**	**Al4**			**3.01405**
Atom	**Atom**	**Length/Å**	**Bond Valence**	**Atom**	**Atom**	**Length/Å**	**Bond Valence**
Al5	O22^{1}	1.813	0.64543	Al6	O16	1.895	0.51713
Al5	O24	1.87	0.55328	Al6	O9^{2}	1.83	0.61645
Al5	O16	1.905	0.50334	Al6	O15	1.854	0.57773
Al5	O18	1.773	0.71912	Al6	O19	1.837	0.60489
Al5	O19	1.793	0.68128	Al6	O20	1.785	0.69617
Al5			**3.10245**	**Al6**			**3.01237**
Atom	**Atom**	**Length/Å**	**Bond Valence**	**Atom**	**Atom**	**Length/Å**	**Bond Valence**
Al7	O22	1.731	0.80556	Al8	O23	1.787	0.69242
Al7	O23	1.765	0.73484	Al8	O23^{1}	1.812	0.64718
Al7	O27	1.793	0.68128	Al8	O24	1.826	0.62315
Al7	O19	1.739	0.78833	Al8	O25	2.058	0.33287
				Al8	O26	1.773	0.71912
Al7			**3.01001**	**Al8**			**3.01473**
Atom	**Atom**	**Length/Å**	**Bond Valence**	**Atom**	**Atom**	**Length/Å**	**Bond Valence**
Pb1	O12	2.225	0.6462	Pb2	O16	2.248	0.61343
Pb1	O13^{3}	2.44	0.39729	Pb2	O18	2.444	0.39372
Pb1	O133	2.44	0.39729	Pb2	O20	2.466	0.3746
Pb1	O13^{1}	2.44	0.39729	Pb2	O17	2.441	0.3964
Pb1	O13^{2}	2.44	0.39729	Pb2	O21	2.643	0.25099
Pb1			**2.23538**	**Pb2**			**2.02913**

Atom	Atom	Length/Å	Bond Valence				
Pb3	O25	2.251	0.60928				
Pb3	O26	2.444	0.39372				
Pb3	O26[1]	2.444	0.39372				
Pb3	O26[2]	2.444	0.39372				
Pb3	O26[3]	2.444	0.39372				
Pb3			**2.18414**				
Atom	**Atom**	**Length/Å**	**Bond Valence**	**Atom**	**Atom**	**Length/Å**	**Bond Valence**
O24	Al5	1.87	0.55328	O14	Al3	1.854	0.57773
O24	Al8	1.826	0.62315	O14	Al1	1.831	0.61478
O24			**1.17643**	**O14**			**1.19251**
Symmetric code: [1]+Y,1/2-X,+Z; [2]1/2-Y,+X,+Z; [3]1/2-X,1/2-Y,+Z							

Table S13. Hydrogen bond parameters for **$Al_{12}Pb_2$**.

D–H···A	d(D–H)	d(H···A)	d(D-A)	∠(D–H···A)
O2–H2···O3	0.95	2.15	2.848(9)	129
C14–H14···O11	1.00	2.50	3.139(5)	121

Table S14. Hydrogen bond parameters for **$Al_{12}Pb_4$**.

D–H···A	d(D–H)	d(H···A)	d(D-A)	∠(D–H···A)
O4–H4···O3	0.95	1.74	2.662(6)	161
C2–H2···O19	1.00	2.45	2.959(8)	111
C5–H5···O16	1.00	2.57	2.931(8)	101
C15–H15···O15	1.00	2.59	2.940(6)	101
C24–H24···O9	0.95	2.40	2.731(16)	100
C26–H26A···O22	0.98	2.02	2.78(2)	134
C27–H27···O20	1.00	2.50	2.968(10)	108
C29–H29C···O2	0.98	2.59	3.336(8)	133
C30–H30···O3	1.00	2.38	3.262(7)	126
C37–H37···O1	0.95	2.53	3.275(9)	136

Table S15. Hydrogen bond parameters for **SAIOC-1**.

D–H···A	d(D–H)	d(H···A)	d(D-A)	∠(D–H···A)
O14–H14···O7	0.95	1.71	2.567(11)	148
O24–H24···O28	0.94	1.77	2.675(7)	162
C4–H4A···O4	0.99	2.02	2.50(3)	107
C15–H15···O7	1.00	2.46	3.266(14)	137
C18–H18···O8	1.00	2.49	3.439(12)	157
C21–H21···O9	1.00	2.57	3.163(10)	118
C28–H28···O2	0.95	2.53	2.902(8)	103
C30–H30B···O1	0.99	2.38	2.82(2)	107
C32–H32A···N2	0.98	2.48	2.95(3)	109
C37–H37···O24	1.00	2.56	3.124(10)	116
C41–H41B···O3	0.99	2.29	3.15(4)	146
C42–H42A···O3	0.99	2.59	3.38(3)	137
C50–H50···O5	0.95	2.55	2.910(11)	103
C50–H50···O5	0.95	2.40	3.209(12)	143